Sparse Approximation-Based Maximum Likelihood Approach for Estimation of Radiological Source Terms

Taewook Lee, *Member, IEEE*, Puneet Singla, *Member, IEEE*, Tarunraj Singh, *Member, IEEE*, and Ajith Gunatilaka

***Abstract*—A computationally efficient and accurate method is presented for identifying the number, intensity and location of stationary multiple radiological sources. The proposed method uniformly grids the region of interest resulting in a finite set of solutions for the source locations. The resulting problem is a sparse convex optimization problem based on $\mathcal{L}_1$-norm minimization. The solution of this convex optimization encapsulates all information needed for the estimation of source terms; the values of the nonzero elements of the solution vector approximates the source intensity, the grid points corresponding to the nonzero elements approximates the source locations, and the number of nonzero elements is the number of sources. The accuracy limited by the resolution of the grid is further improved by making use of the maximum likelihood estimation approach. The performance of sparse approximation based maximum likelihood estimation is verified using real experimental data acquired from radiological field trials in the presence of up to three point sources of gamma radiation. The numerical results show that the proposed approach efficiently and accurately identifies the source terms simultaneously, and it outperforms existing methods which have been used for stationary multiple radiological source terms estimation.**

***Index Terms*—Maximum likelihood estimation, parameter estimation, radiation monitoring, radioactive materials.**

I. Introduction

IN RECENT years, the threats from chemical, biological, radiological and nuclear (CBRN) incidents have increased [1]. They include lost or stolen radioactive material, and covert release from unknown locations. Furthermore, covert transfer of radiological material can use air, water and land based vehicles, consequently mandating the development of technology to detect the sources in real-time. In an incident, between May 1996 and April 1997, many servicemen were exposed to radiation caused by $^{137}C_s$ and $^{60}C_o$ [2] at the Lilo Training Detachment of Frontier Troops, which is located 25 km east of Tbilisi, the capital of Georgia. Eleven soldiers were accidentally overexposed to radiological radiations and showed symptoms for clinical manifestation of radiation effects mainly of the skin. Some of the victims were reported to suffer from "chronic radiation disease from uneven external fractionated irradiation." These sources were later (September 1997) found in different parts of the grounds of the Lilo Centre, including the scrapyard and the soccer field. A coat pocket of a uniform was the location of a source with the highest dose rate.

The risk of exposure to radiological materials has increased in recent years, and the exposure has led to increased radiation-caused critical illness or even death. There have been 99 accidents at nuclear power plants from 1952 to 2009, totaling 20.5 billion in property damages (defined as incidents that either resulted in the loss of human life or more than 50,000 of property damage) [3], [4]. Fifty-seven accidents have occurred since the Chernobyl disaster, and almost two-thirds (56 out of 99) of all nuclear-related accidents have occurred in the USA. More broadly, this threat also potentially exists due to chemical, biological and nuclear incidents. During the deliberate or unintentional release of toxic material, the number of contaminated civilians could exponentially increase depending on the large quantities, high intensities and long period of release time of the toxic materials. Consequently, when hazardous materials such as radiological sources are released and detected, rapid and accurate response for the isolation of the hazardous materials is required. This is accomplished by identifying the number of sources and characterizing the location and intensity of the sources. Furthermore, the uncertainties associated with the estimates of the source parameters are required to be determined in order to reduce false alarms.

The challenge of identifying the source parameters and estimating the uncertainties associated with the calculated source parameters is relevant due to the absence of densely sited sensors which can only measure the intensity of the sources in the region of interest. Furthermore, when there exists two or more sources, the mean radiation count at a sensor is the sum of mean radiation counts due to all sources. Hence, sensor models that mathematically approximate a relation between the sensor measurements and the source parameters are necessary and these models result in uncertainties associated with the estimates of the source parameters. When the mapping between the sensor measurements and the source parameters is non-linear and involves probabilistically-modeled background radiation, it poses a unique challenge for the radiological source terms estimation.

Many methods have been exploited for the radiological source term estimation, including least squares approaches [5], [6], [7], heuristic optimization methods [8] such as genetic

Manuscript received December 26, 2013; revised August 06, 2014; accepted January 17, 2016. Date of current version April 15, 2016.

T. Lee, Engineer, Member IEEE, is with Samsung, Korea (e-mail: twlee2@buffalo.edu).

P. Singla and T. Singh are with the Dept. of Mechanical & Aerospace Engineering, University at Buffalo, Buffalo, NY-14260 (e-mail: psingla@buffalo.edu, tsingh@buffalo.edu).

A. Gunatilaka is with the Land Division, Defence Science and Technology Group, 506 Lorimer Street Fishermans Bend, VIC 3207, Australia (e-mail: Ajith.Gunatilaka@dsto.defence.gov.au).

Digital Object Identifier 10.1109/TNS.2016.2520255

algorithms and simulated annealing, and Bayesian methods such as particle filters [9], [10]. The least squares approach or other gradient based optimization methods use the residues (error between the measurement and the predicted measurement) to modify the source parameters by solving the problem until the residues are reduced to within a specified tolerance. The resulting non-convex optimization problem is conventionally solved based on a selected gradient based optimization algorithm. A drawback of these approaches, which is common to all gradient based approaches used to solve non-convex optimization problems, is that the solution can converge to local minima rather than the global minima, depending on the initial estimate of the source parameters. Heuristic optimization methods such as genetic algorithm and simulated annealing do not require gradient information, thus they are more likely to converge to global minima than gradient based optimization algorithms. However, these methods are computationally expensive and consequently are poor choices for real-time applications. Furthermore, they have the tendency to fit the noise present in sensor data and also do not provide any measure of confidence in their estimates.

An alternative to simply fitting the measurement data is to exploit sensor noise characteristics. A simplistic probabilistic approach is to provide source estimates which maximizes the likelihood probability of measurement data. This leads to the well-known Maximum Likelihood Estimation (MLE) approach which leads to a nonlinear optimization problem [9], [11]. Like the least square approach and the heuristic optimization algorithms, the MLE just provides a point estimate for source parameters and does not provide any information regarding the confidence in those estimates. The Bayesian methods such as the particle filter use the Bayes' rule where a prior distribution is combined with the information contained in the measurements to give a posterior probability density function (pdf). In Refs. [9], [12], [11], the authors have discussed the application of sequential Monte Carlo method for the radiological source parameter estimation. In particular, the Importance Sampling with Progressive Correction (ISPC) algorithm has been proposed for radiological source term estimation. The ISPC is a class of particle filtering [13] and a Bayesian technique which assumes that a prior distribution is available for source parameter estimation. Our knowledge of the likelihood function is then combined with the prior information to yield the posterior probability density function (pdf). In general, the prior information is assumed to be available for the source parameters, and all information about the source parameters is contained in the posterior pdf of the parameters. However, computation of the posterior mean to obtain the estimates of the parameters is difficult and hence it is necessary to consider approximations. This is a common problem which arises in Bayesian framework based estimation and many numerical methods exist for approximating the posterior mean. Ristic et al., [9] have proposed using one such method named ISPC for the radiological source parameters estimation. The basic idea is that approximation of the posterior mean via ISPC involves drawing samples of the parameter vector from an importance density which is a known density from which random samples can be drawn, and approximating the integral by a weighted sum of the samples. The importance density can be simply replaced by the prior. However, it has been suggested that the straightforward use of the prior as the importance density would not work well because it can be expected that the prior will often be far more diffuse than the likelihood [9]. As a result many, or even all, samples will be drawn in undesirable parts of the parameter space and estimates of the source parameters will be poor. Instead it is proposed to use a multi-stage procedure in which samples are obtained from a series of posterior distributions which becomes progressively closer to the true posterior distribution. The idea is that the posterior distribution approximations used in the early stages should be simpler to obtain samples from than the true posterior distribution.

Although these approaches have been successful in estimating source parameters, a major drawback of all these approaches is that they are not directly conducive to the determination of the number of sources. Assuming different number of sources, they seek the most suitable candidate which maximize the likelihood of measurements. Under a certain model selection criterion such as Bayesian Information Criterion (BIC) [14], [15], assumed different number of sources are compared to choose the best match to the measurement by solving numerous optimization problems. Ristic et al., have proposed the use of model selection criterion for estimating the number of sources along with their location and intensities [9]. The main idea of their approach is to exhaustively compare different models of possible numbers of sources while making use of model selection criterion such as the BIC. Many model selection criteria have been proposed in the literature [16], and selection of the best model depends on the criterion used. All model selection criteria are a compromise between model complexity and the model accuracy. Here, model complexity is given by the number of independent parameters in the model which are proportional to the number of sources. The exhaustive comparison-based multiple source estimation method needs to solve a parameter estimation problem under each and every hypothesis and then choose the best hypothesis under a model selection criterion. This is not suited for large numbers of sources and generally require a good a-priori information on the number of sources.

In conclusion, the radiological source term estimation problem deals with the following three factors: (1) a nonlinear sensor model which involves probabilistically-modeled background radiation, (2) sensor measurements which are random variables and obey a Poisson distribution, (3) characterization of the uncertainties associated with the sensor model. These problems require development of accurate and computationally efficient methods which can identify the radiological source parameters such as the number, location and intensities of the sources and characterize the uncertainties associated with the estimates of the source parameters.

The goal of the proposed source term estimation algorithm is to accurately determine the number of sources and precisely estimate other source parameters such as locations and intensities and characterize the uncertainties associated with these estimates. *Sparse Convex Optimization Problem based Maximum Likelihood Estimation* (SCOPMLE) makes use of sparse approximation tools to determine the number of sources

which serves as the initial guess for the source intensity and locations when solving the maximum likelihood problem, to obtain an accurate estimate of the source intensity and location with the associated confidence quantification. The main idea is to discretize the space where radiation sources potentially exist which is tantamount to asserting that the sources have to lie at the vertices of the grid. Since the location of grid points (potential source locations) is prescribed, the only unknown in the nonlinear sensor model is the source strength which appears linearly, transforming the problem into a linear one in source intensity [17], [18]. The number of sources along with the source parameters such as source location and intensity are inferred from the intensity distribution which has a sparse property assuming that the number of sources is less than the number of grid points (potential sources). The sparse convex optimization is a pre-processing step which exploits $\mathcal{L}_1$-norm minimization to determine the number of sources and estimates of the other source parameters. The subsequent maximum likelihood estimation process refines the solution to develop a more precise estimate of the source locations and intensities. A key advantage of the proposed method is that it handles model selection and parameter estimation at the same time as identifying the number of sources along with source locations and intensities. Both numerical simulations and experiment data are used to show the efficacy of the proposed ideas and the results obtained are compared against those obtained by conventional maximum likelihood algorithm and ISPC based sequential Monte Carlo method. In all the considered cases, the proposed approach was able to find the global maximum which maximizes the probability of matching the observed set of data.

The structure of paper is as follows: first a model for radiological sensor is presented followed by the description of the details of the proposed source identification approach. Finally, experimental results are presented to illustrate the efficacy of the proposed ideas.

II. Problem Formulation

The goal of the source term estimation algorithm is to provide estimates for source parameters: location, intensity and the number of sources along with associated uncertainty bounds. There are different ways to represent uncertainty associated with source parameter estimates such as worst-case scenarios attempting to provide bounds using interval analysis, methods based on fuzzy set theory, evidence theory, which tries to create upper and lower bounds on the likelihood of events, and probabilistic or stochastic models, which offer mathematically the richest structure. Probabilistic means of representing uncertainties have been explored extensively and provides the greatest wealth of knowledge which is exploited in this work [19], [20], [21]. The first step in source term estimation is to develop a mathematical model relating the measured quantities to source parameters.

A. Sensor Model

A Geiger-Müller counter is a radiation sensor and is chosen to be used as a sensor model [9] in this research work. According to the sensor model, the mean radiation count at location (x_j, y_j) due to N_s number of point sources is given as:

$$b_j = \sum_{k=1}^{N_s} \frac{\omega_k}{(x_k - x_j)^2 + (y_k - y_j)^2} + \omega_0 \tag{1}$$

where, x_k and y_k are the unknown coordinates of the k^{th} point source location and ω_k represents the unknown intensity of the k^{th} point source. ω_0 is the mean background radiation due to environmental effects present at the sensor location in the absence of actual radiation source and is assumed to be constant over the domain of interest. The actual sensor measurement z_j^i at sensor location (x_j, y_j) is assumed to obey a Poisson distribution [22], [23], whose variance is equal to the mean radiation count. Note that the superscript i is an index to reflect multiple measurements collected at the same location. Assuming the radiation measurements are independent random variables, the joint likelihood function at the j^{th} location can be written as:

$$L(\mathbf{z}_j|b_j) = \prod_{i=1}^{m} e^{-b_j} \frac{b_j^{z_j^i}}{z_j^i!} \tag{2}$$

where m is the total number of sensor readings at location (x_j, y_j). Notice that the true radiation count b_j due to N_s number of sources is both the mean and variance of this Poisson distribution.

Given the sensor model and the radiation dose measurements, the goal of the point source term estimation problem is to identify the source parameter vector denoted as $\boldsymbol{\theta}_k = [x_k, y_k, \omega_k]^T$, $k = 1, \ldots, N_s$, and the number of sources, N_s from b_j, $j = 1, \ldots, M$, where M is the number of sensors located in the region of interest.

III. Sparse Convex Optimization Problem based Maximum Likelihood Estimation (SCOPMLE) Approach

As discussed in Section I, many algorithms have been proposed in the literature for the radiological source estimation. Most existing multiple source estimation methods [9], [11] assume that the number of sources is known and the source estimation is then essentially a parameter estimation problem, generally formulated as a maximum likelihood estimation problem or a Bayesian estimation problem as discussed in the previous section. When multiple sources are to be identified in the absence of the exact prior information on the number of sources, the number of sources needs to be determined along with source locations and intensities, which poses a unique challenge for source estimation algorithms. In this section, an approach is developed to estimate the number of sources along with the source intensity and location. Sparse approximation formulation is exploited to determine the number of unknown sources. The proposed work is an extension of our prior work presented in [17], [18]. First, the key idea is explained by assuming that perfect radiation count measurements are available at the sensor location. Later, the basic idea is extended to the case of imperfect measurements assuming the measurement distribution to be Poisson distribution.

A. Perfect Measurements

The main idea is to discretize the space where the radiation sources potentially exist. The motivation is that the source locations x_k and y_k can only take on a finite set of known values and the sensor model of Eq. (1) is a linear model in source intensity. Let us consider the potential radiation sources to be located on a two-dimensional grid consisting of a total of N node points, (x_k^G, y_k^G), $k = 1, \ldots, N$. One choice of (x_k^G, y_k^G) is a fine grid over the region of interest. The grid need not be uniform, so another choice would be a fine mesh in regions of particular interest, such as densely populated areas, and a coarser mesh over other regions. Prior knowledge about the source distribution, if available, greatly reduces the number of grid points. Assuming the radiation source to lie on grid node, (x_k^G, y_k^G), the true radiation count given by Eq. (1) as a function of ω_k yields:

$$b_j = \sum_{k=1}^{N} \omega_k a_{kj}(x_k^G, y_k^G, x_j, y_j) + \omega_0,$$
$$a_{kj} = \frac{1}{(x_k^G - x_j)^2 + (y_k^G - y_j)^2},\ j = 1, 2, \cdots, M \tag{3}$$

where M is the number of sensors, and ω_0 is background radiation measured in the absence of any radiological source, and the only unknowns in the above equation are ω_k. Since b_j is linear in the source intensity, Eq. (3) can be rewritten as:

$$\mathbf{b} = \mathbf{A}\Omega + \omega_{\mathbf{0}} \tag{4}$$

where, $\mathbf{b} = \{b_1, b_2 \cdots, b_M\}^T$ is a $M \times 1$ vector of sensor observations and $\mathbf{A}$ is given as:

$$\mathbf{A} = \begin{bmatrix} \frac{1}{(x_1^G - x_1)^2 + (y_1^G - y_1)^2} & \cdots & \frac{1}{(x_N^G - x_1)^2 + (y_N^G - y_1)^2} \\ \vdots & \ddots & \vdots \\ \frac{1}{(x_1^G - x_M)^2 + (y_1^G - y_M)^2} & \cdots & \frac{1}{(x_N^G - x_M)^2 + (y_N^G - y_M)^2} \end{bmatrix} \tag{5}$$

The observation matrix $\mathbf{A}$ is $M \times N$ fully determined by sensor locations and the grid locations and $\omega_{\mathbf{0}}$ is a vector of dimension $M \times 1$ with every element being ω_0. This discretization process allows for direct estimation of the source intensity distribution on grid points. The sources can now be fully represented by an $N \times 1$ vector $\Omega = \{\omega_1, \omega_2, \cdots, \omega_N\}^T$, such that the element ω_i indicates the intensity of a potential source at (x_i^G, y_i^G). By definition, $\omega_i \geq 0$ and an actual source is located at (x_i^G, y_i^G) only when ω_i exceeds a certain threshold. The number of the elements in Ω exceeding the threshold is the number of point sources over the region (N_s). In a case of real incident there are likely to be a very limited number of discrete sources, many fewer than the available spatial grid points, i.e., N is much greater than number of sources N_s. Hence, the great majority of components ω_i will be equal to zero or in other words, Ω is a sparse vector. In the case of a widely distributed source the assumption of sparsity would not hold. The present methods are limited to discrete sources, in which a single spatially compact source, or small number, are to be detected.

It should be noted that size of $\mathbf{A}$ is $M \times N$ with $N > M$ in general and hence Ω cannot be uniquely determined from $\mathbf{b}$. There are an infinite number of Ω which satisfy Eq. (4). The best solution then should be the one that achieves the best tradeoff between the sparsity of Ω and the magnitude of the residual vector $\mathbf{A}\Omega - \mathbf{b} - \omega_{\mathbf{0}}$, which is characterized by a selected norm. With the sparsity of Ω and the measure of residuals defined, the following sparse optimization problem can be defined to estimate the source parameters:

$$\min \quad \|\Omega\|_0 \tag{6}$$
$$\text{subject to} \quad \mathbf{A}\Omega = \mathbf{b} - \omega_{\mathbf{0}} \tag{7}$$
$$\Omega \geq 0 \tag{8}$$

where $\|\cdot\|_0$ refers to the 0-norm which is the total number of nonzero elements in the vector. Note that the 0-norm minimization problem is a non-convex optimization problem. However, it has been shown that one can approximate the solution to this sparse approximation problem by a sequence of convex problem [24], [25]. The $\mathcal{L}_1$-norm also produces relatively sparse vectors when minimized, and is convex. In order to apply the powerful tools of convex analysis, therefore, the minimization problem to be addressed is formulated as follows:

$$\hat{\Omega} = \min_{\Omega} \|\mathbf{D}\Omega\|_1 \tag{9}$$
$$\text{subject to } \mathbf{A}\Omega = \mathbf{b} - \omega_{\mathbf{0}} \tag{10}$$
$$\Omega \geq 0 \tag{11}$$

In the original $\mathcal{L}_1$-norm minimization problem in [26], the matrix A in the constraint Eq. (10) is assumed to be a matrix of unit column vectors. The normalized version of $\mathbf{A}$ is used in the problem definition, given by $\hat{\mathbf{A}} = \mathbf{A}\mathbf{D}^{-1}$, where $\mathbf{D}$ is the diagonal matrix of the 2-norms of the columns of $\mathbf{A}$. This sparsity-seeking property is of interest in various applications; compressed sensing, error correction, image processing, and so on [26], [27], [28]. Furthermore, an iterative $\mathcal{L}_1$-norm minimization, originally proposed in [26], can be used to get closer to actual 0-norm solution. The basic idea of this approach is that the algorithm consists of solving a sequence of weighted $\mathcal{L}_1$-norm minimization problems where the weights used for the next iteration are computed from the value of the current solution [29]. The algorithm is presented in Table I. In step 3, ϵ is a small positive number introduced to avoid "divide by zero" problem in practice. Each iteration of the algorithm simply requires solving $\mathcal{L}_1$-norm minimization problem, and hence, it can be implemented readily using convex optimization tools. In [29], it has been shown that this iterative approach outperforms $\mathcal{L}_1$-norm minimization in the sense that fewer measurements are needed for an exact sparse solution. Nonetheless, note that there is no absolute guarantee that the sparsest solution can be found by using this iterative scheme but it helps improve the sparsity of the solution. This approach has recently been used for the design of over-complete code books for communication systems [26] and in our prior work [18], we make use of these tools to find unknown source parameters.

TABLE I
RE-WEIGHTED $\mathcal{L}1$-NORM MINIMIZATION ALGORITHM

1) Set the iteration count l to zero and $w_i^{(0)} = 1$, $i = 1, ..., N$.
2) Solve the weighted $\mathcal{L}_1$-norm minimization problem:

$$\hat{\Omega}^{(l)} = \min_{\Omega} \|W^{(l)}\mathbf{D}\Omega\|_1 \qquad (12)$$

$$, W^{(l)} = \text{diag}(w_i^{(l)}) \text{subject to } \mathbf{A}\Omega = \mathbf{b} - \omega_0$$
$$\Omega \geq 0$$

3) Update the weights: for each $i = 1, ..., N$,

$$w_i^{(l+1)} = \frac{1}{|\Omega_i^{(l)}| + \epsilon} \qquad (13)$$

4) Terminate when the variation in the cost in sequential iteration is below a threshold Δ or when l reaches a specified maximum number of iterations
l_{max}. Otherwise, increment l and go to step 2.

B. Imperfect Measurements

In this section, this sparse approximation scheme is extended for the realistic scenario where measurement distribution function is assumed to be Poisson distribution. Given a sample of m measured values z_j^i, $i = 1, \ldots, m$, at each sensor location (x_j, y_j), the maximum-likelihood value of the mean radiation count b_j, is computed. Furthermore, the variance of the estimates for b_j is computed to express the confidence associated with the estimate of b_j. Later on, the iterative $\mathcal{L}_1$-norm minimization approach is modified to make use of mean and variance estimates for b_j.

Assuming the radiation measurements are independent random variables, the joint density of the measurement vector $\mathbf{z}_j = [z_j^1, \ldots, z_j^m]^T$ conditional on the parameter vector $\boldsymbol{\theta}$ can be written as Equation (2). The MLE estimate represented by $\hat{b}_j$ corresponds to the value of the mean radiation count at sensor location which maximizes the likelihood function $L(\mathbf{z}_j|b_j)$. Since the likelihood function is positive and involves exponential of a quantity, the MLE problem is equivalent to maximizing the log-likelihood function, $\log[L(\mathbf{z}_j|b_j)]$:

$$\begin{aligned}\hat{b}_j &= \arg\max_{b_j} \log\left[L\left(\mathbf{z}_j|b_j\right)\right] \qquad (14)\\ &= \arg\min_{b_j} \left\{-\log L\left(\mathbf{z}_j|b_j\right)\right\}\\ &= \arg\min_{b_j} \left\{\sum_{i=1}^{m} \left(b_j - z_j^i \log b_j + \log z_j^i!\right)\right\}\end{aligned}$$

Taking the first derivative of cost function and equating it to zero yields the following solution for $\hat{b}_j$:

$$\hat{b}_j = \frac{1}{m}\sum_{i=1}^{m} z_j^i \qquad (15)$$

Notice that $\hat{b}_j$ is an unbiased estimator for b_j, i.e., $\mathrm{E}[\hat{b}_j] = b_j$. Furthermore, the confidence in this estimate can be expressed by computing the variance associated with $\hat{b}_j$:

$$\sigma_j^2 = \mathrm{E}\left[\left(\hat{b}_j - b_j\right)^2\right] = \mathrm{E}\left[\left(\frac{1}{m}\sum_{i=1}^{m}\left(z_j^i - b_j\right)\right)^2\right] = \frac{b_j}{m} \qquad (16)$$

It should be mentioned that this variance is also equal to the Cramèr-Rao bound and hence the MLE estimate for b_j is an optimal estimate. As expected, the variance in the estimate of b_j decreases by increasing the number of observations, i.e., $\hat{b}_j$ becomes a more efficient estimate of b_j as the number of observations increases. It should be noted that we assume stationarity of the background which can be violated if there is a precipitation event during the measurement, or if the duration of measurment is very long. Now the observation error constraint of Eq. (10) can be replaced by the following constraint:

$$\|\mathbf{A}\Omega - \hat{\mathbf{b}}\|_2^2 \leq C\|\Sigma\|_2^2 \qquad (17)$$

where,

$$\hat{\mathbf{b}} = \left\{\frac{1}{m_1}\sum_{i=1}^{m_1} z_1^i, \frac{1}{m_2}\sum_{i=1}^{m_2} z_2^i, \cdots, \frac{1}{m_{\mathrm{M}}}\sum_{i=1}^{m_M} z_M^i\right\} \qquad (18)$$

$$\Sigma = \{\sigma_1^2, \sigma_2^2, \cdots, \sigma_M^2\}^T \qquad (19)$$

where m_j represents the number of measurements of the j^{th} sensor. C is greater than one and represents how much error one can tolerate in observation satisfaction. This plays an important role since a lower value of C will correspond to over-fitting imperfect observations and higher value of C will correspond to large error in explaining sensor observations. Furthermore, it is expected that the value of the variance $\|(\hat{\mathbf{A}}\hat{\Omega} - \hat{\mathbf{b}})\|_2^2$ would be large when the true sources are not located at any grid points which can be addressed by picking a larger value for C. Now, the optimal estimate $\hat{\Omega}$ is defined as the solution to the following $\mathcal{L}_1$ norm minimization problem:

$$\begin{aligned}&\text{minimize} && \|\mathbf{D}\boldsymbol{\Omega}\|_1\\ &\text{subject to} &&\\ &&& \|\mathbf{A}\Omega - \hat{\mathbf{b}}\|_2^2 \leq C\|\Sigma\|_2^2\\ &&& 0 \leq \Omega \qquad (20)\end{aligned}$$

which will be referred to as SCOP (Sparse Convex Optimization Problem). As discussed earlier, the sparsity of the solution to the problem given by Eq. (20) can be enhanced using an iterative re-weighting scheme as described in Table I. The minimization problem is solved iteratively using the problem formulation given by Eq. (20), with the new cost function given by

$$\hat{\Omega}^{(l+1)} = \arg\min_{\Omega} \sum_{i=1}^{N} \frac{\hat{\Omega}_i}{\hat{\Omega}_i^{(l)} + \epsilon} \qquad (21)$$

where $\hat{\Omega}^{(l+1)}$ is the optimal estimate in the $(l+1)^{th}$ iteration, $\hat{\Omega}_i^{(l)}$ is the i^{th} element of the optimal estimate from the $(l)^{th}$ iteration, and ϵ is a small positive number introduced to avoid the "divide by zero" problem. Since the optimizer will never return an exact zero for non-existing source at grid points, ϵ is also used as the threshold to identify the existence of a source.

C. Reducing Estimation Errors by Maximum Likelihood Estimator

There is no absolute guarantee that the sparsest solution can be found by using the iterative re-weighting scheme, and the accuracy of estimation is limited by the resolution of the grid.

In other words, the grid points defined as "true sources" may not be located at the true source locations. A maximum likelihood estimator is further used to reduce the error between the estimated parameters and the true parameters. Maximum likelihood estimation (MLE) yields estimates for the unknown quantities which maximize the probability of obtaining the observed set of data.

The MLE estimate represented by $\hat{\boldsymbol{\theta}}$ corresponds to the value of the parameter vector $\boldsymbol{\theta} = [\theta_1, \boldsymbol{\theta}_2, \cdots, \boldsymbol{\theta}_{N_s}]^T$ being estimated which maximizes the likelihood function of Eq. (2). Since the likelihood function is positive and involves exponential of a quantity, the MLE problem is equivalent to maximizing the log-likelihood function, $\log[L(\mathbf{z}|\boldsymbol{\theta})]$:

$$\hat{\boldsymbol{\theta}}_{MLE} = \arg\max_{\hat{\boldsymbol{\theta}}} \log[L(\mathbf{z}|\boldsymbol{\theta})] = \arg\min_{\hat{\boldsymbol{\theta}}} \{-\log L(\mathbf{z}|\boldsymbol{\theta})\} \tag{22}$$

subject to source strengths being non-negative, i.e.,

$$\omega_k \geq 0,\ k = 1, 2, \cdots, N_s \tag{23}$$

It should be noticed that the constraint equation is imposed for better conditioning of the MLE problem. Ideally, one can solve for $\hat{\boldsymbol{\theta}}$ by equating the first derivative of MLE cost-function to zero and verifying that the second derivative is negative at the optimal solution. However, due to the nonlinear nature of resulting equations and the non-negativity constraint of Eq. (23) on the source strength, the MLE problem is solved with the help of numerical methods such as MATLAB built-in routine *fmincon*. In [9] and [11], the MLE approach has been used to find estimates for source parameters assuming the number of sources to be known. It is well known that the MLE problem leads to nonlinear system of equations to be solved which are very sensitive to initial guess for source parameter values. Instead of randomly choosing the initial searching points which may result in wrong estimates, it is proposed here to choose the sparse solution obtained by solving the problem of Eq. (20) as the initial values to find the parameters which maximize the likelihood function given by Eq. (2).

D. Cramér-Rao Bound

In addition to the point estimates, one is also interested in obtaining some measure of confidence in those point estimates. Generally, the variance or covariance matrix is used as a measure of confidence for point estimates. However, in the absence of a closed-form solution for the resulting MLE problem, a closed-form expression for the covariance matrix does not exist. In this section, the concept of Cramèr-Rao bound is discussed which can be used to provide a lower bound on the covariance matrix of any unbiased estimator. This can be useful for the investigation of the quality of a particular estimator such as a maximum likelihood estimator and particle filtering.

The Cramér-Rao bound (CRB) states that the inverse of the Fisher information matrix is a lower bound on the expected errors between estimated states and true states. For an unbiased estimator $\hat{\boldsymbol{\theta}}$ of $\boldsymbol{\theta}$, the CRB is given by [30]:

$$E\left[(\hat{\boldsymbol{\theta}} - \boldsymbol{\theta})(\hat{\boldsymbol{\theta}} - \boldsymbol{\theta})^T\right] \geq \mathbf{F}^{-1} \tag{24}$$

where $\mathbf{F}$ is the Fisher information matrix which is usually derived from the information metric [30] and measures the amount of information the measurement vector $\mathbf{z}$ carries about the unknown parameter vector $\boldsymbol{\theta}$. It is defined as:

$$\mathbf{F} = -E\left\{\frac{\partial^2}{\partial\boldsymbol{\theta}\partial\boldsymbol{\theta}^T}\log[L(\mathbf{z}|\boldsymbol{\theta})]\right\} \tag{25}$$

with the likelihood function $L(\mathbf{z}|\boldsymbol{\theta})$ given by Eq. (2). Expanding the log likelihood function yields:

$$\begin{aligned}\log[L(\mathbf{z}|\boldsymbol{\theta})] &= \sum_{j=1}^{M}\sum_{i=1}^{m}\log\left(e^{-b_j(\boldsymbol{\theta})}\frac{b_j(\boldsymbol{\theta})^{z_j^i}}{z_j^i!}\right)\\ &= \sum_{j=1}^{M}\sum_{i=1}^{m}\Big(\log(e^{-b_j(\boldsymbol{\theta})}) + z_j^i\log(b_j(\boldsymbol{\theta}))\\ &\quad - \log(z_j^i!)\Big)\end{aligned} \tag{26}$$

Since the last term is independent of $\boldsymbol{\theta}$, it can be written as a constant K:

$$\log[L(\mathbf{z}|\boldsymbol{\theta})] = K + \sum_{j=1}^{M}\sum_{i=1}^{m}\left\{z_j^i\log(b_j(\boldsymbol{\theta})) - b_j(\boldsymbol{\theta})\right\} \tag{27}$$

Now, computing the derivative of $\log[L(\mathbf{z}|\boldsymbol{\theta})]$ yields:

$$\frac{\partial\log[L(\mathbf{z}|\boldsymbol{\theta})]}{\partial\boldsymbol{\theta}} = \sum_{j=1}^{M}\sum_{i=1}^{m}\left[z_j^i\frac{1}{b_j(\boldsymbol{\theta})}\frac{\partial b_j(\boldsymbol{\theta})}{\partial\boldsymbol{\theta}} - \frac{\partial b_j(\boldsymbol{\theta})}{\partial\boldsymbol{\theta}}\right] \tag{28}$$

$$\begin{aligned}\frac{\partial^2\log[L(\mathbf{z}|\boldsymbol{\theta})]}{\partial\boldsymbol{\theta}\partial\boldsymbol{\theta}^T} &= \sum_{j=1}^{M}\sum_{i=1}^{m}\left[z_j^i\frac{-1}{(b_j(\boldsymbol{\theta}))^2}\frac{\partial b_j(\boldsymbol{\theta})}{\partial\boldsymbol{\theta}^T}\frac{\partial b_j(\boldsymbol{\theta})}{\partial\boldsymbol{\theta}}\right.\\ &\quad \left. + \frac{z_j^i}{b_j(\boldsymbol{\theta})}\frac{\partial^2 b_j(\boldsymbol{\theta})}{\partial\boldsymbol{\theta}\partial\boldsymbol{\theta}^T} - \frac{\partial^2 b_j(\boldsymbol{\theta})}{\partial\boldsymbol{\theta}\partial\boldsymbol{\theta}^T}\right]\end{aligned} \tag{29}$$

Making use of the gradient operator $\nabla_{\boldsymbol{\theta}} \triangleq \partial/\partial\boldsymbol{\theta}$, we can rewrite the aforementioned relations as:

$$\begin{aligned}\frac{\partial^2\log[L(\mathbf{z}|\boldsymbol{\theta})]}{\partial\boldsymbol{\theta}\partial\boldsymbol{\theta}^T} &= \sum_{j=1}^{M}\sum_{i=1}^{m}\left[\nabla_{\boldsymbol{\theta}}\nabla_{\boldsymbol{\theta}}^T b_j(\boldsymbol{\theta})\left(\frac{z_j^i}{b_j(\boldsymbol{\theta})} - 1\right)\right.\\ &\quad \left. - \nabla_{\boldsymbol{\theta}} b_j(\boldsymbol{\theta})\nabla_{\boldsymbol{\theta}}^T b_j(\boldsymbol{\theta})\frac{z_j^i}{b_j^2(\boldsymbol{\theta})}\right]\end{aligned} \tag{30}$$

Substituting Eq. (30) into Eq. (25) leads to

$$\begin{aligned}\mathbf{F} = -E\left[\sum_{j=1}^{M}\sum_{i=1}^{m}\left\{\nabla_{\boldsymbol{\theta}}\nabla_{\boldsymbol{\theta}}^T b_j(\boldsymbol{\theta})\left(\frac{z_j^i}{b_j(\boldsymbol{\theta})} - 1\right)\right.\right.\\ \left.\left. - \nabla_{\boldsymbol{\theta}} b_j(\boldsymbol{\theta})\nabla_{\boldsymbol{\theta}}^T b_j(\boldsymbol{\theta})\frac{z_j^i}{b_j^2(\boldsymbol{\theta})}\right\}\right]\end{aligned} \tag{31}$$

Since $E[z_j^i] = b_j(\boldsymbol{\theta})$, the first term in the braces becomes zero and it results in

$$\mathbf{F} = \sum_{j=1}^{M}\sum_{i=1}^{m}\frac{\nabla_{\boldsymbol{\theta}} b_j(\boldsymbol{\theta})\nabla_{\boldsymbol{\theta}}^T b_j(\boldsymbol{\theta})}{b_j(\boldsymbol{\theta})} \tag{32}$$

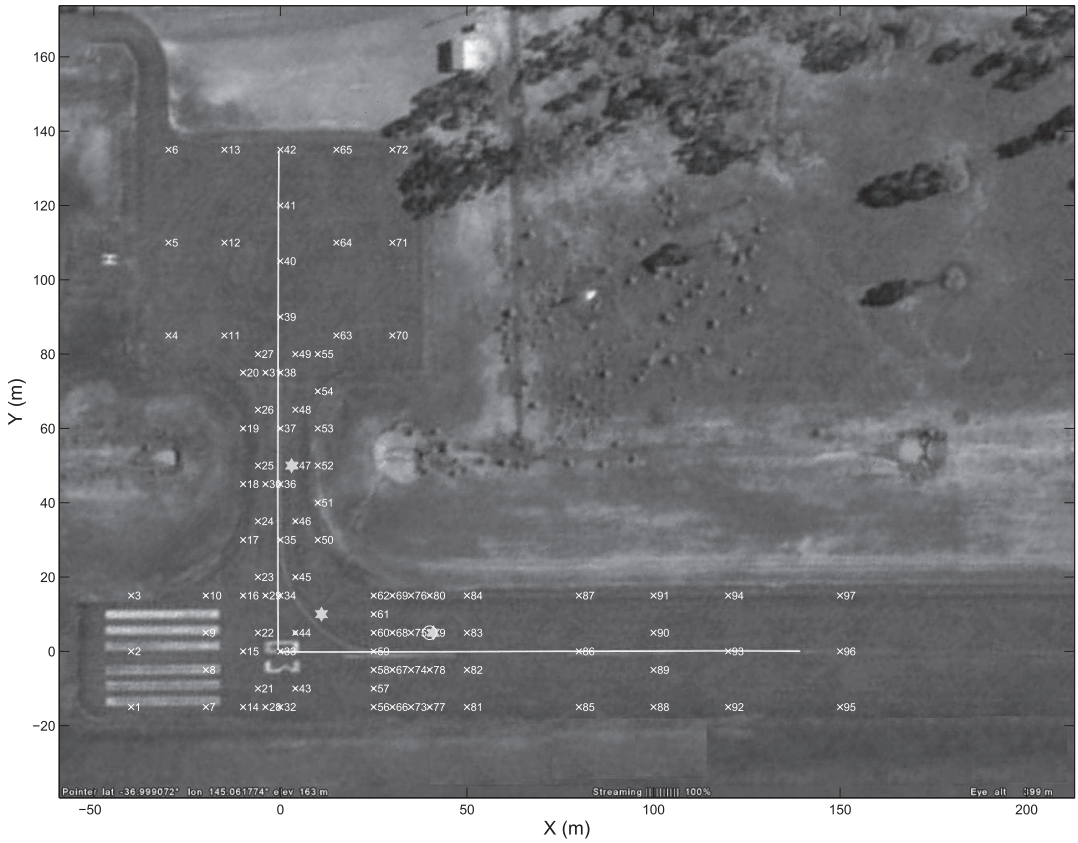

Fig. 1. Aerial image of the site where the field trial was conducted with Sources marked as grey stars.

TABLE II
RADIOLOGICAL SOURCE LOCATIONS

Test set	Source 1	Source 2	Source 3
1	(11, 10)m	-	-
2	(11, 10)m	(3, 50)m	-
3	(11, 10)m	(3, 50)m	(41, 5)m

TABLE III
RADIOLOGICAL SOURCE INTENSITIES

Source	Type	Activity (MBq)
1	$^{137}\mathrm{C_s}$	26×10^3
2	$^{137}\mathrm{C_s}$	5×10^3
3	$^{60}\mathrm{C_o}$	0.2×10^3

Finally, the required partial derivatives are given as:

$$\frac{\partial b_j(\boldsymbol{\theta})}{\partial x_k} = \frac{2\omega_k(x_j - x_k)}{\left((x_j - x_k)^2 + (y_j - y_k)^2\right)^2} \tag{33}$$

$$\frac{\partial b_j(\boldsymbol{\theta})}{\partial y_k} = \frac{2\omega_k(y_j - y_k)}{\left((x_j - x_k)^2 + (y_j - y_k)^2\right)^2} \tag{34}$$

$$\frac{\partial b_j(\boldsymbol{\theta})}{\partial \omega_k} = \frac{1}{(x_j - x_k)^2 + (y_j - y_k)^2} \tag{35}$$

The theoretical CRB are computed as the square-root values of diagonal elements of $\mathbf{F}^{-1}$ (which correspond to the lower bounds of estimation error standard deviations) for real experimental data.

IV. NUMERICAL RESULTS BASED ON REAL EXPERIMENTAL DATA

In this section, real experimental data is considered to illustrate the performance of the proposed sparse approximation based MLE algorithm and its performance is compared with both the conventional MLE and ISPC algorithms. The experimental data was acquired during radiological field trials in the presence of up to three stationary sources of gamma radiation as described in Ref. [11], [12]. The number of sources is assumed to be known a-priori for the implementation of the conventional MLE and ISPC algorithms, however one can identify them using the exhaustive model order selection methods as explained in Ref. [9].

TABLE IV
TEST 1: INITIAL ESTIMATE FOR SOURCE PARAMETERS

		True	Guess 1	Guess 2	Guess 3	Guess 4
Source 1	x(m)	11	1	50	-50	0.5
	y(m)	10	1	80	80	0.5
	intensity	9105	1000	1000	1000	1000

TABLE V
TEST 2: INITIAL ESTIMATE FOR SOURCE PARAMETERS

		True	Guess 1	Guess 2	Guess 3	Guess 4
Source 1	x(m)	11	1	20	1	50
	y(m)	10	1	20	1	80
	intensity	9105	1000	1000	1000	1000
Source 2	x(m)	3	20	1	50	1
	y(m)	50	20	1	80	1
	intensity	1868	1000	1000	1000	1000

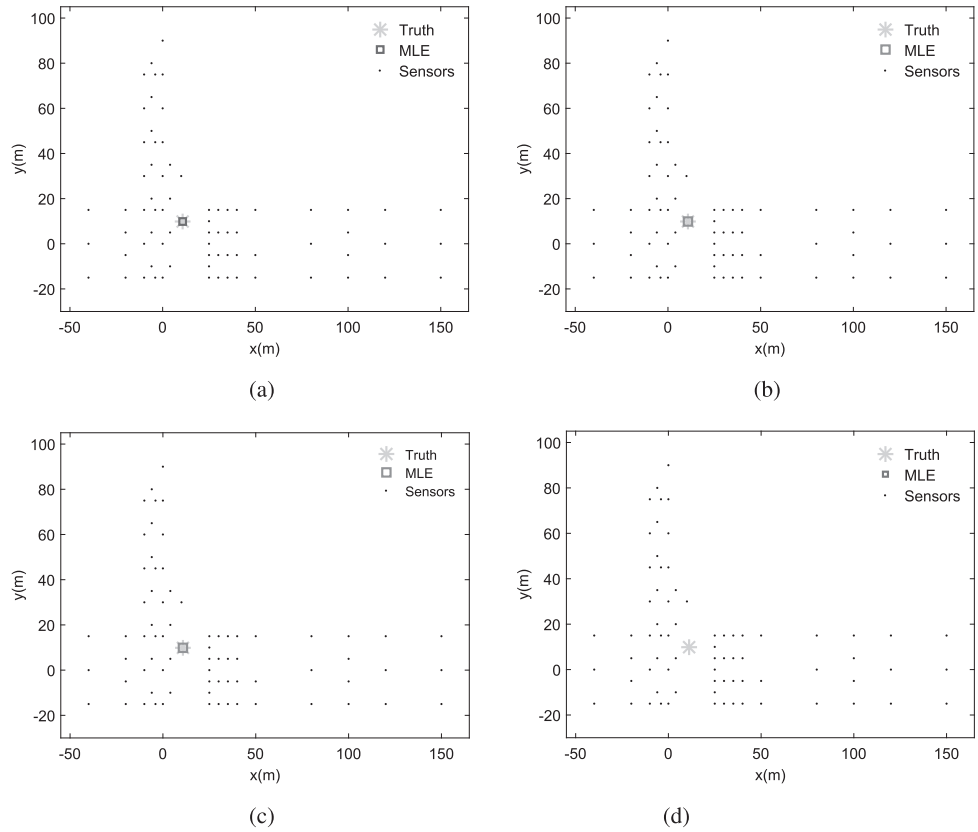

Fig. 2. Test 1: Performance of MLE for four different initial guesses (a) Initial Guess 1: MLE converged (b) Initial Guess 2: MLE converged (c) Initial Guess 3: MLE converged (d) Initial Guess 4: MLE diverged outside the area shown.

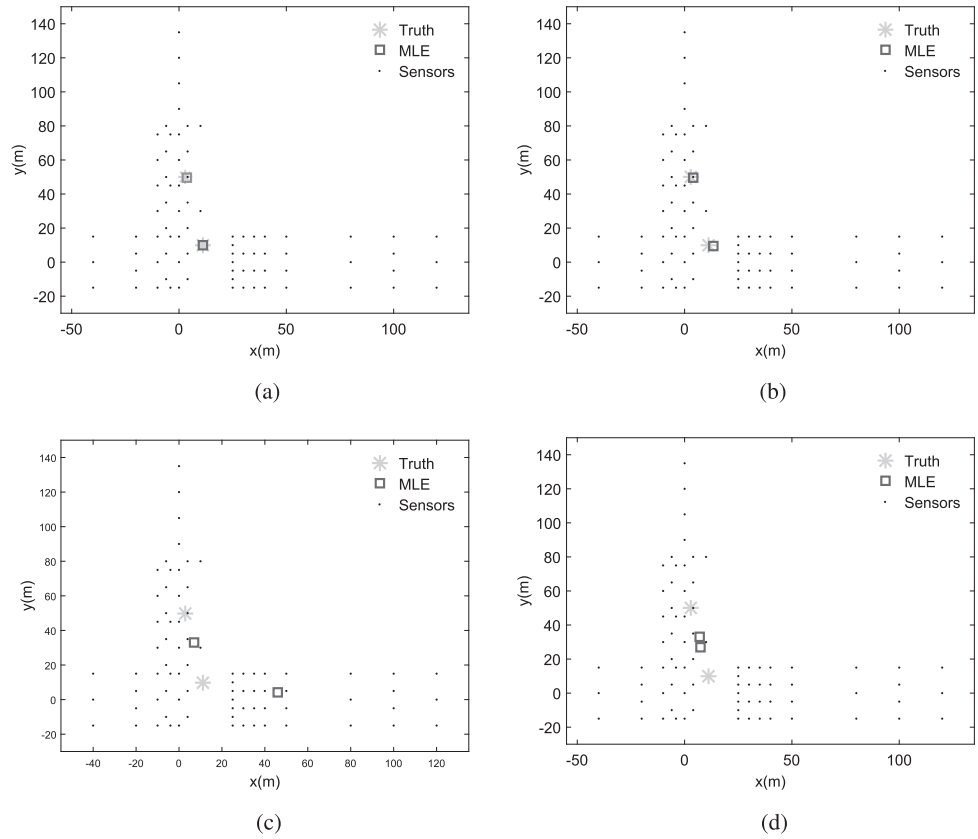

Fig. 3. Test 2: Performance of MLE for four different initial guesses (a) Initial Guess 1: MLE Converged (b) Initial Guess 2: MLE Converged (c) Initial Guess 3: MLE Converged to local minima (d) Initial Guess 4: MLE Converged to local minima.

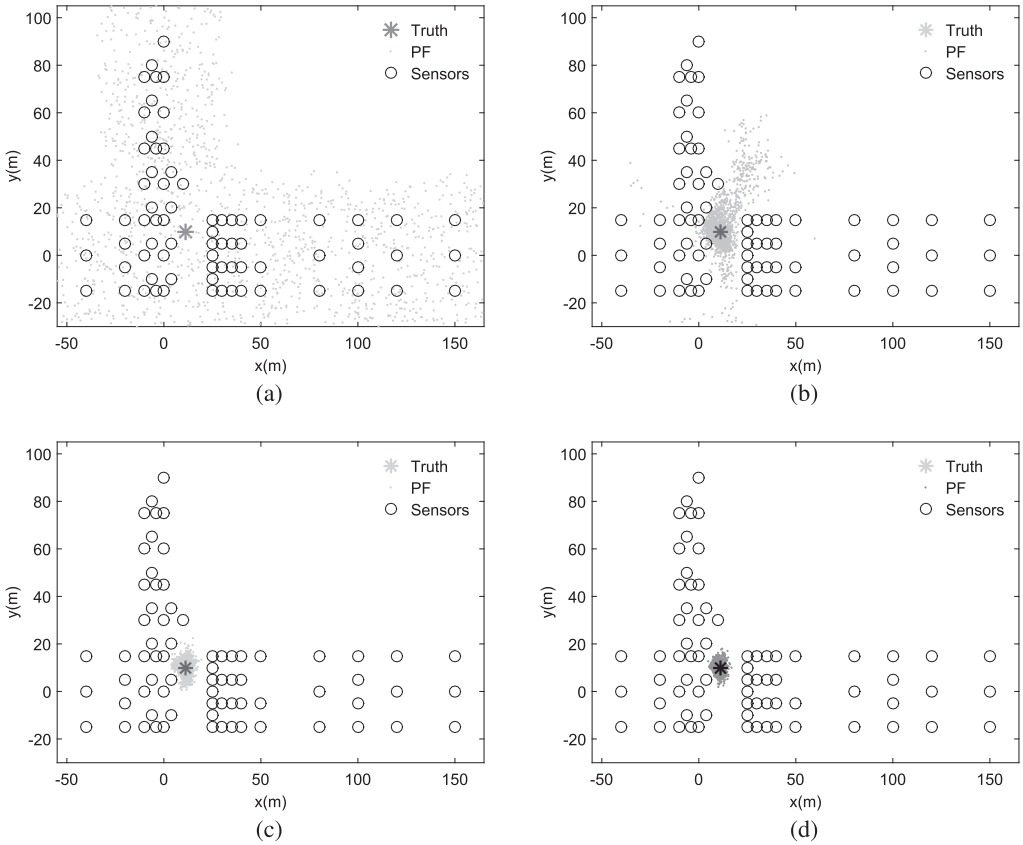

Fig. 4. Test 1: A single run of ISPC (a) Stage 1, (b) Stage 3, (c) Stage 5, and (d) Stage 7.

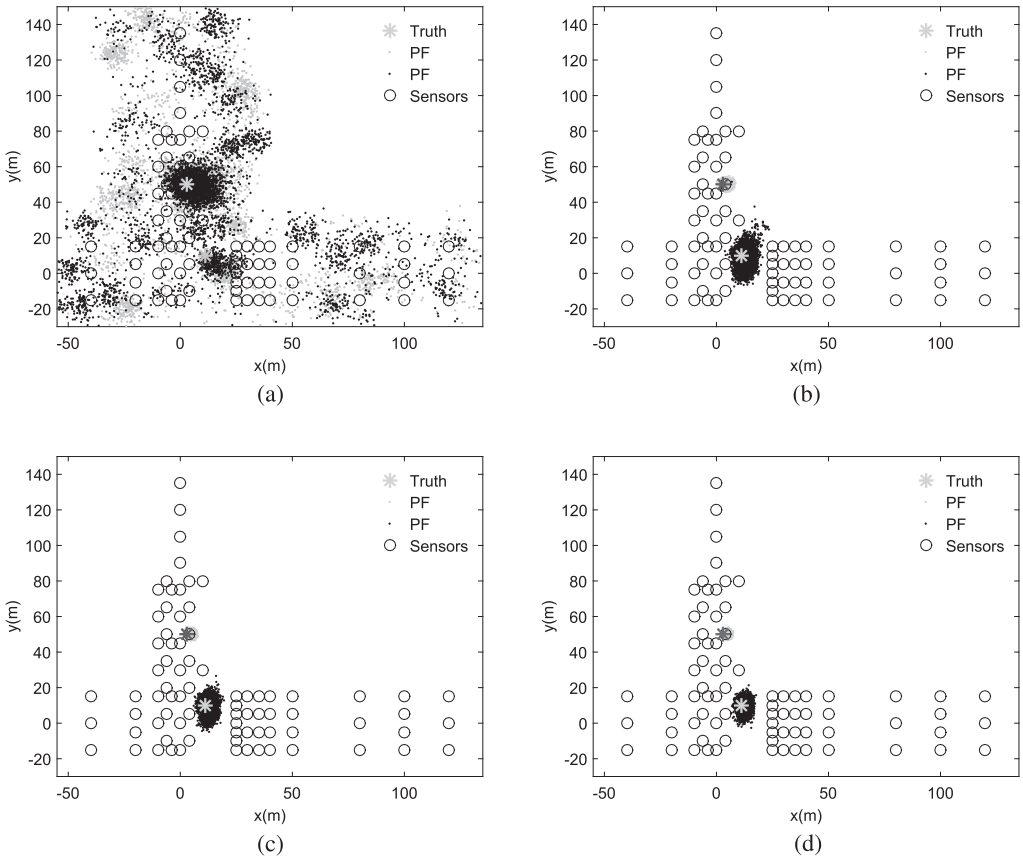

Fig. 5. Test 2: A single run of ISPC (a) Stage 2, (b) Stage 5, (c) Stage 7, and (d) Stage 9.

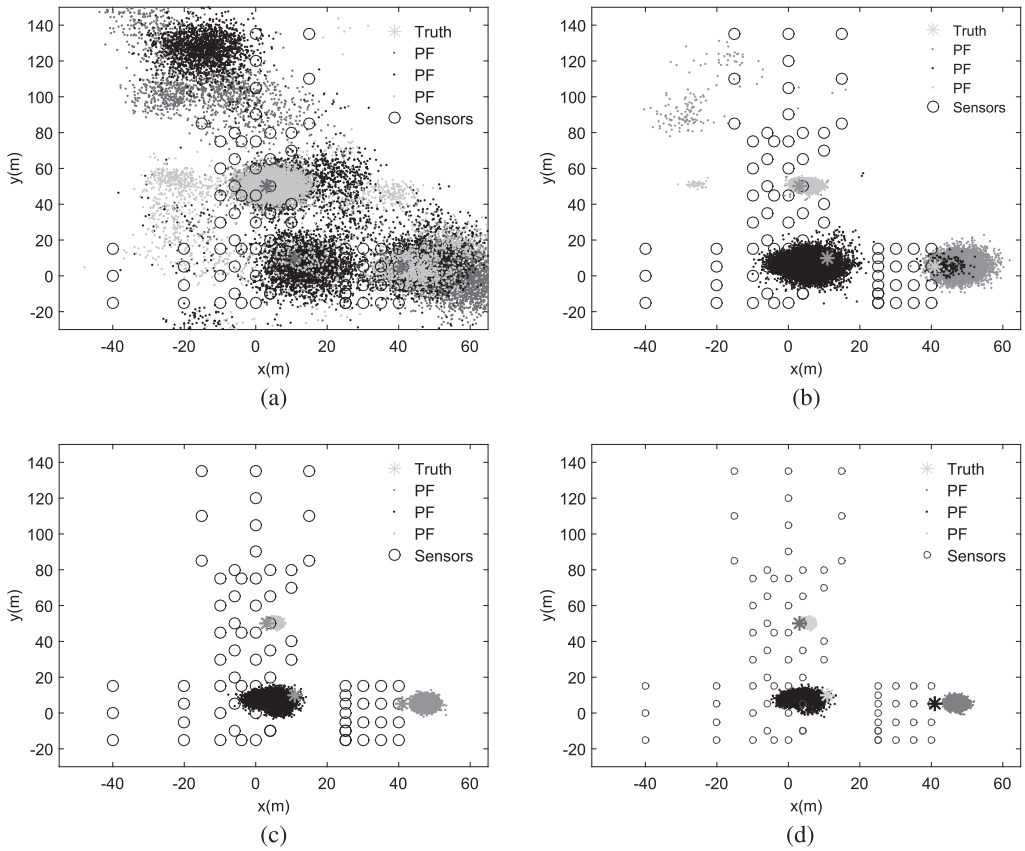

Fig. 6. Test 3: A single run of ISPC (a) Stage 3, (b) Stage 5, (c) Stage 7, and (d) Stage 12.

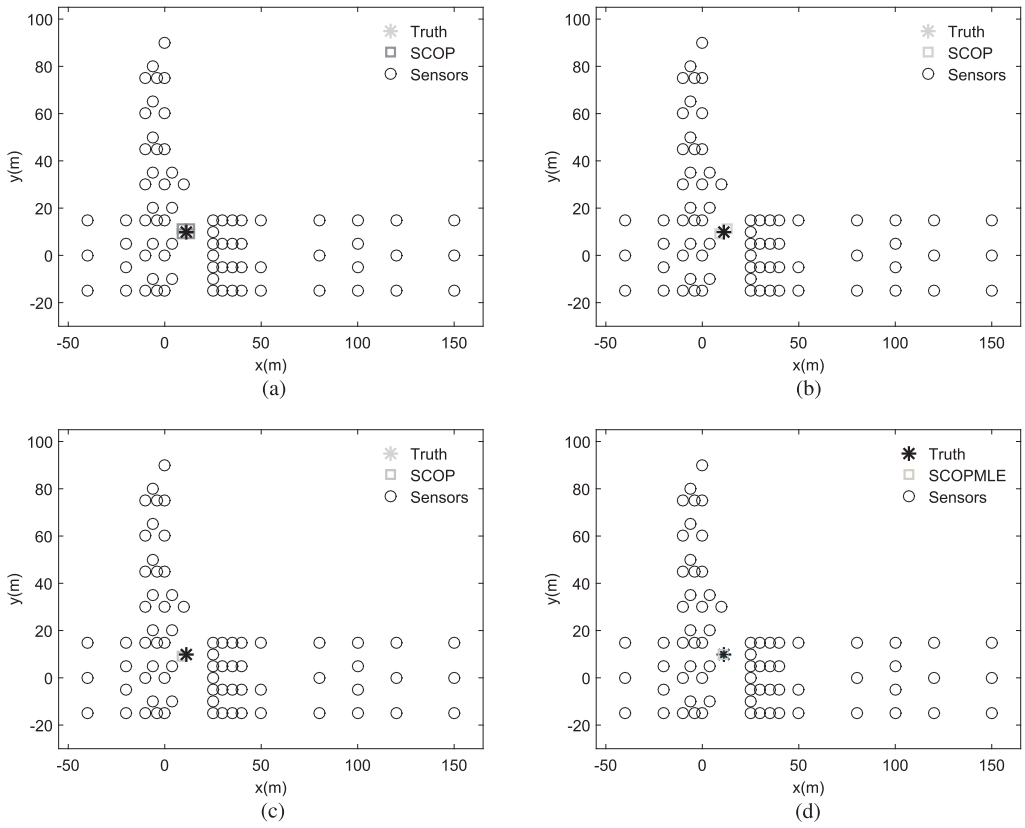

Fig. 7. Test 1: Performance of SCOPMLE (a) 1st iteration, (b) 2nd iteration, (c) 4th iteration, and (d) SCOPMLE.

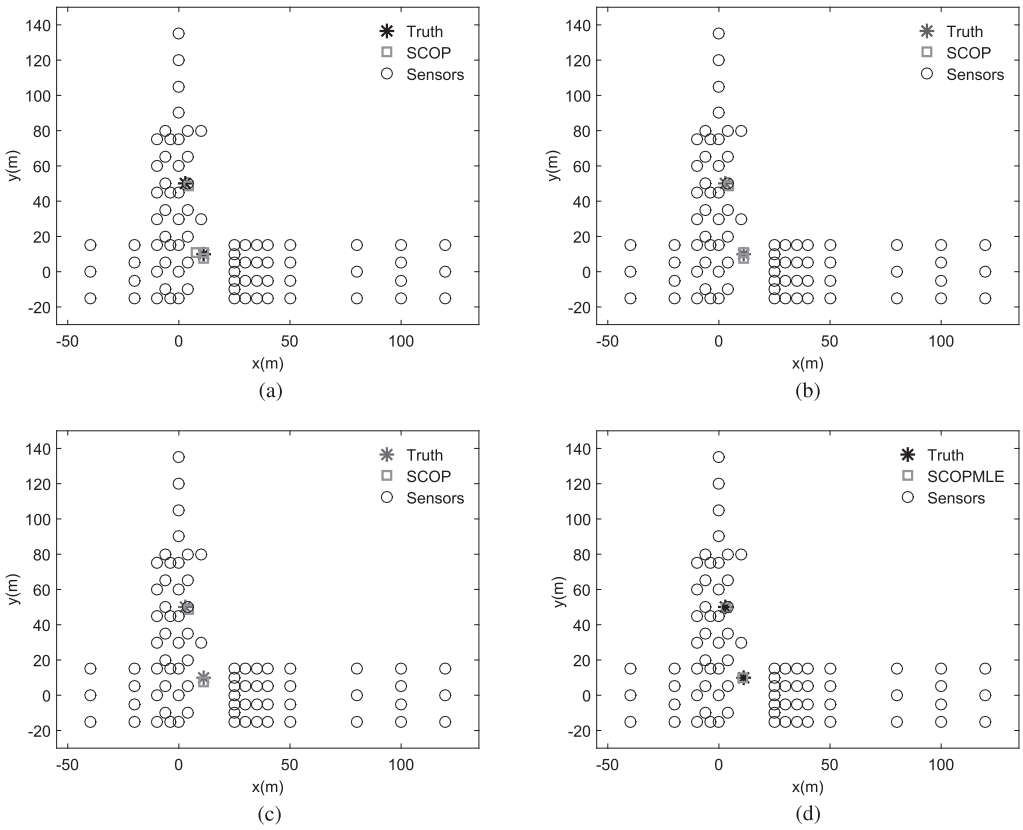

Fig. 8. Test2: Performance of SCOPMLE (a) 1st iteration, (b) 2nd iteration, (c) 4th iteration, and (d) SCOPMLE.

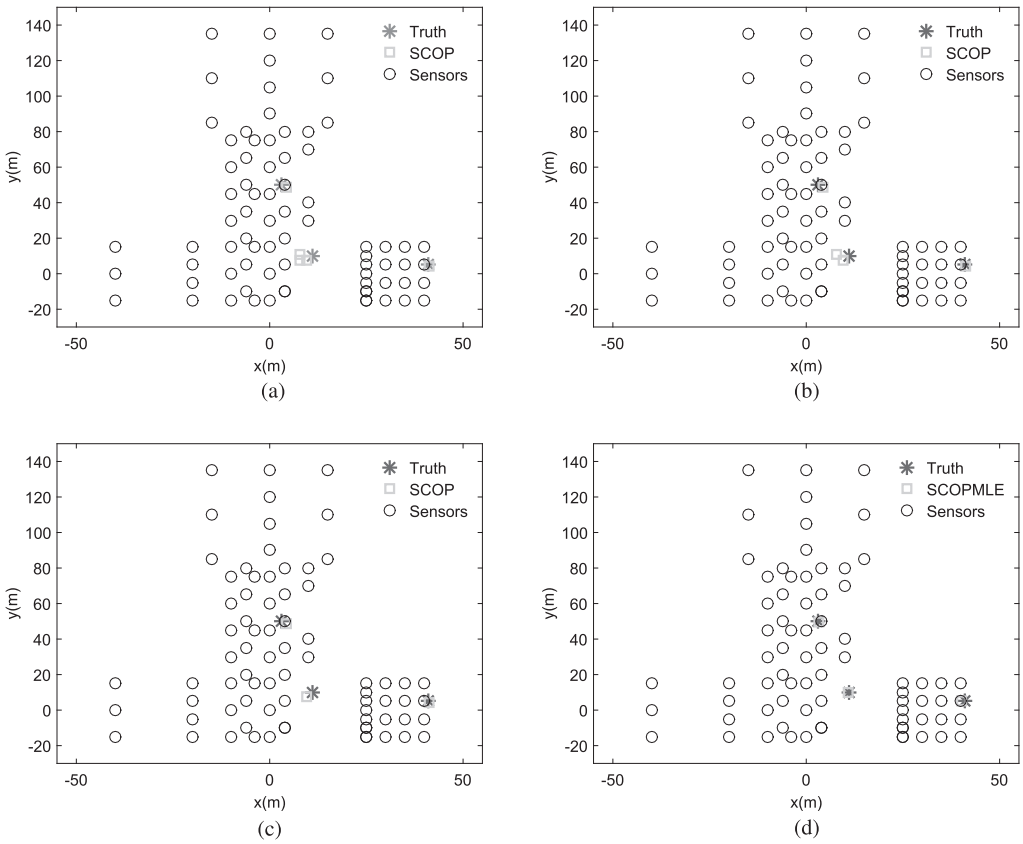

Fig. 9. Test3: Performance of SCOPMLE (a) 1st iteration, (b) 2nd iteration, (c) 4th iteration, and (d) SCOPMLE.

A. Experimental-Data Details

Radiation dose measurements at spatially distributed sensors were collected with one (Test 1), two (Test 2) and three (Test 3) radiation point sources, respectively. The aerial image of the site where the field trial was conducted is shown in Fig. 1; the grey star indicates source locations, and the numbered white grid point marked with a cross indicates the sensor locations. Note that a single sensor mounted on a cart was moved from location to location, which precludes modeling detector-to-detector variations. The measurement dose rate was converted to measurement count with a conversion factor of $1/0.21$, which accounted for the efficiency of the sensor. More details of the data collection and processing is provided in the paper [31]. Sixty independent count dose measurements at each sensor location were collected with time interval of one second. In the absence of any sources present, radiation dose measurements were collected in order to measure the background radiation level which obeys Poisson distribution with mean 0.9 counts [11],i.e., $\omega_0 \approx 0.9$. The locations and intensities of the true radiological sources in the field trials are given in Tables II and III, respectively. Although the sources are typically characterised in terms of their activity in GBq, in this work, for simplicity, we represent the strength of a radiation point source by the expected count rate at a distance of 1 meter from the source. Based on this characterization, the strengths of the three radiation sources calibrated in this manner were 9105, 1868 and 467, for Sources 1, 2, and 3, respectively.

B. Conventional MLE

The conventional MLE estimates were obtained numerically for all three test cases by making use of the procedure listed in Ref. [11]. The MATLAB function *fmincon* is used to solve the resulting optimization problem. Since in nonconvex optimization problems the solution can converge to local minima based on the initial estimate for the source parameters, it is required to run MLE with different initial estimate to verify its performance. Four different initial estimates are selected and they are given in Tables IV and V. The corresponding results are obtained via 100 Monte Carlo runs executed in MATLAB. The *randperm* command is used to select 20 unique samples by a random permutation of the 60 samples collected at each sensor location without replacement, for the Monte Carlo runs, and are shown in Fig. 2 and 3 for Test 1 and Test 2, respectively; the dots indicate the sensor locations, the grey stars mark the true source locations and squares indicate the estimated source locations by the MLE algorithm. The MLE converged to the true solution for Test 1 when initialized with the first three initial guesses listed in Table IV, but diverged when initial guess 4 was used. The MLE converged to the true solution for Test 2 with the first guess, converged close to the truth for the second and to local optima when initialized with the three and fourth initial guesses listed in Table V. For Test 3, the scenario with three sources, MLE diverged on every single run to a location outside the search area of interest and the results are not shown. In the presence of three sources, the MLE diverges on every single run which is consistent with results reported in Ref. [11]. In conclusion, when the initial guess is reasonably close to the truth, the algorithm converges to the truth, and its convergence properties deteriorate as the number of sources increases and the initial guess is not close to the truth.

C. Importance Sampling with Progressive Correction (ISPC)

Assuming that the prior knowledge of where the sources potentially exist is available, the prior probability mass function $\pi_0(\boldsymbol{\theta})$ for the source location is assumed to be a uniform distribution. The value of the samples for the source intensity is drawn from a Gamma distribution with shape parameter $k = 1.5$ and scale parameter $v = 8000$ [11]. This Gamma distribution supports that the initial source intensity value can be drawn from $[0, \infty)$, and it is broad enough to cover all likely non-negative source intensity values.

ISPC is initialized by drawing random samples in $3N_s$ dimensional parameter space from $\pi_0(\boldsymbol{\theta})$. The number of samples is set to $N = 2500N_s$ [11], and the expansion factors are evenly distributed on a log scale as discussed in Ref. [12]. The following termination criterion for ISPC proposed in Ref. [11] has been used:

$$\sum_{i=1}^{N_s} \sqrt{\sigma_{x_i}^2 + \sigma_{y_i}^2} \leq 2.5N_s \tag{36}$$

A single run of ISPC for Test 1, Test 2 and Test 3 is shown in Figs. 4, 5 and 6, respectively. A unique color is assigned to random particles associated with each source sampled from the random distribution $\pi_0(\boldsymbol{\theta})$. The different color blobs illustrate the agglomeration of these particles over the true source location, as the algorithm progresses. From these figures, it is clear that samples converge to the true source locations as number of iterations increases. Especially, the result for Test 3, with three sources present, indicates that ISPC is a suitable algorithm to identify three sources parameters, while MLE diverges. These results are once again consistent with results reported in Ref. [11].

From these results, it is clear that the ISPC algorithm works well in estimating the unknown source parameters and one can also compute the corresponding posterior density function associated with those estimates. However, the particle filter based approach is not suitable for estimating the number of sources present when only radiation counts are provided. One generally needs to depend upon exhaustive model selection criteria like Bayesian information criteria to guess the number of sources which can be computationally very expensive.

D. Sparse Convex Optimization Problem based Maximum Likelihood Estimation (SCOPMLE)

This section describes the paradigm where the SCOP solution is generated using the approach outlined in Table I. This solution forms the initial guess for a MLE and the combination of SCOP and MLE is what will be referred to as SCOPMLE. A uniform 50×50 grid of potential source locations is generated over the region of interest for Test 1, Test 2, and Test 3. The grid is assumed to be fine enough to cover the region with sufficient resolution. No grid point is located at a sensor location in order

TABLE VI
TEST 1: SCOPMLE VS. MLE VS. ISPC

		True	MLE $\pm \sigma$	ISPC $\pm \sigma$	SCOP	SCOPMLE $\pm \sigma$
Source 1	x(m)	11	10.64 $\pm$ 0.38	10.53 $\pm$ 0.36	9.00	**10.64 $\pm$ 0.38**
	y(m)	10	9.77 $\pm$ 0.43	9.42 $\pm$ 0.43	9.18	**9.77 $\pm$ 0.43**
	intensity	9105	8898 $\pm$ 302	8918 $\pm$ 303	3771	**8898 $\pm$ 302**

TABLE VII
TEST 2: SCOPMLE VS. MLE VS. ISPC

		True	MLE $\pm \sigma$	ISPC $\pm \sigma$	SCOP	SCOPMLE $\pm \sigma$
Source 1	x(m)	11	11.28 $\pm$ 0.32	10.42 $\pm$ 0.31	11.20	**10.68 $\pm$ 0.34**
	y(m)	10	9.76 $\pm$ 0.49	9.22 $\pm$ 0.46	7.47	**9.90 $\pm$ 0.44**
	intensity	9105	8565 $\pm$ 315	8472 $\pm$ 338	5054	**8820 $\pm$ 321**
Source 2	x(m)	3	3.49 $\pm$ 0.36	4.38 $\pm$ 0.73	4.43	**3.37 $\pm$ 0.39**
	y(m)	50	49.71 $\pm$ 0.62	48.57 $\pm$ 0.10	48.86	**49.72 $\pm$ 0.62**
	intensity	1868	2046 $\pm$ 168	2252 $\pm$ 376	2608	**1819 $\pm$ 163**

TABLE VIII
TEST 3: SCOPMLE VS. MLE VS. ISPC

		True	MLE $\pm \sigma$	ISPC $\pm \sigma$	SCOP	SCOPMLE $\pm \sigma$
Source 1	x(m)	11	-	10.32 $\pm$ 0.36	9.65	**10.78 $\pm$ 0.34**
	y(m)	10	-	9.21 $\pm$ 0.45	7.47	**9.72 $\pm$ 0.44**
	intensity	9105	-	8423 $\pm$ 410	3053	**9008 $\pm$ 377**
Source 2	x(m)	3	-	4.53 $\pm$ 0.52	4.39	**3.28 $\pm$ 0.32**
	y(m)	50	-	48.26 $\pm$ 0.10	48.86	**49.63 $\pm$ 0.60**
	intensity	1868	-	2354 $\pm$ 279	4369	**1806 $\pm$ 154**
Source 3	x(m)	41	-	42.25 $\pm$ 1.66	41.24	**40.24 $\pm$ 0.96**
	y(m)	5	-	3.91 $\pm$ 2.31	4.28	**5.08 $\pm$ 2.78**
	intensity	467	-	610 $\pm$ 312	775	**356 $\pm$ 163**

to avoid the singularity problem of the sensor model given by Eq. (1). The matrix $\mathbf{A}$ in Eq. (20) is $M \times N$, i.e., 73×2500, 78×2500 and 75×2500 for Test 1, Test 2 and Test 3, respectively and is fully determined by the grid points and the sensor locations. The diagonal matrix $\mathbf{D}$ with the diagonal elements given by the $\mathcal{L}_2$-norms of the matrix $\mathbf{A}$ is then easily obtained, and its size is $N \times N$, i.e., 2500×2500.

Based upon our experience, the value of C is set to be 5^4 and is fixed for each test. And the value of the threshold ϵ in the iterative re-weighting scheme of Eq. (21) is set to be 1 and hence only $\omega_k > 1$ count/sec at a distance of 1 meter, is considered to be sources. For implementation, CVX for MATLAB [32], a package for solving convex optimization problems is used. Among many different exit conditions in the use of CVX, only "Solved" condition is accepted. During iterative $\mathcal{L}_1$-norm minimization, the value of the cost function (costF) is computed, and the following termination criteria is implemented:

$$|costF(l+1) - costF(l)| < (\Delta = 0.00005) \qquad (37)$$

where $costF(l+1)$ and $costF(l)$ are values of the cost function in the $(l+1)^{th}$ iteration and in the $(l)^{th}$ iteration, respectively.

Figs. 7, 8, and 9 illustrate the number of sources and their locations as the number of iterations are increased in the proposed re-weighted $\mathcal{L}_1$-norm minimization for Test 1, Test 2, and Test 3, respectively. It is clear from these results the sparse convex optimization problem (SCOP) accurately identifies the number of sources in each test case and provides a reasonable estimate of source location. Furthermore, source parameter estimates along with one σ bounds for different algorithms are provided in Tables VI, VII, and VIII for Test 1, Test 2 and Test 3, respectively. From these results it is clear that the SCOP accuracy, which is limited by resolution of the grid, is highly improved by making use of the maximum likelihood approach and using SCOP estimates as initial guess. It is also clear that SCOPMLE provides consistent estimates for uncertainty associated with source parameter estimates. For all the three test cases, the true source parameters lie inside one σ box around SCOPMLE estimates. In this sense, the proposed approach even outperforms ISPC. Graphically, σ ellipse bounds in 3-dimensional space which captures the true source parameters (represented by the oval ellipsoid located away from the center of the σ box) are shown in Fig. 10.

Finally, the execution time of SCOPMLE is compared to that of MLE and ISPC in the MATLAB environment on a laptop computer (Windows 7 Home Premium, 2.2 GHz Intel processor, 4 GB RAM). The MATLAB function TICTOC is used to get the execution times of different algorithms implemented and the results are given in Table IX. The execution time of MLE, ISPC and SCOPMLE is mainly determined by the initial estimate, the number of samples and the grid size, respectively. It can be seen that the execution time for SCOPMLE is the shortest compared to the other methods. MLE does not converge in the presence of three sources, and the execution time for ISPC increases dramatically with the number of sources, mainly because high-dimensional space requires high number of samples. SCOPMLE does not scale the grid size for each Test and performs with good balance between accuracy and computational efficiency for radiological source term estimation.

V. PERFORMANCE STUDY

It is evident that numerous physical experimental parameters such as SNR, number of sensors, relative location of sensors,

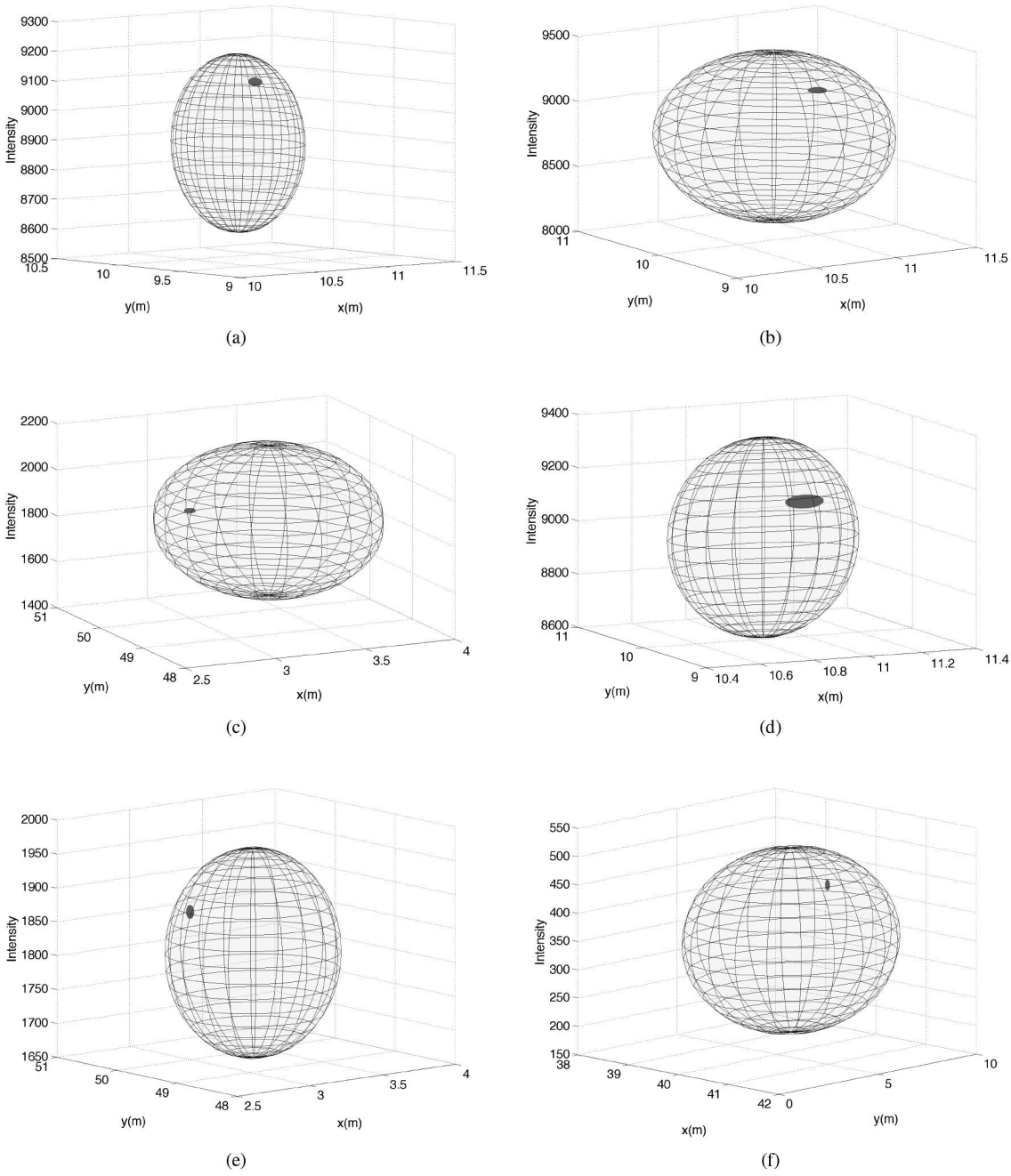

Fig. 10. σ ellipse bounds (a) Test 1: Source 1, (b) Test 2: Source 1, (c) Test 2: Source 2, (d) Test 3: Source 1, (e) Test 3: Source 2, and (f) Test 3: Source 3.

etc., and algorithmic parameters such as convergence threshold, grid size, etc., influence the performance of any source estimation algorithm. In this section we evaluate the impact of source strength threshold ϵ, mean background noise and signal-to-noise ratio (SNR) on the performance of the proposed SCOPMLE algorithm. The impact of grid size on the performance of the SCOPMLE is also evaluated. The results of these tests are described in this section.

The source strength threshold variable ϵ is used to assert the existence or non-existence of a source at a grid location, and is deemed an important variable that can impact the performance of the SCOPMLE in correctly identifying the number of sources. Numerical studies conducted by varying ϵ from 10^{-3} to 10^{2} revealed that the algorithm consistently identified the same number of sources, and has no impact on the estimate of the source parameters. This was due to the fact that the $\mathcal{L}_1$ norm minimization problem reduced the source strength at most of the grid point to the machine numerical precision of zero. The following subsections describe the performance of SCOPMLE when the mean background noise is assumed to be unknown and the impact of SNR.

TABLE IX
EXECUTION TIME (SEC): SCOPMLE VS. MLE VS. ISPC

	MLE	ISPC	SCOP	SCOPMLE
Test 1	18	342	11	**16**
Test 2	80	1560	13	**48**
Test 3	-	5100	16	**85**

TABLE X
SOURCE PARAMETER ESTIMATION WITHOUT ANY KNOWLEDGE OF MEAN BACKGROUND NOISE

		True	Test Case 1 $\pm$ σ	Test Case 2 $\pm$ σ	Test Case 3 $\pm$ σ
Source 1	x(m)	11	10.72 $\pm$ 0.30	10.78 $\pm$ 0.31	10.83 $\pm$ 0.33
	y(m)	10	9.79 $\pm$ 0.41	9.89 $\pm$ 0.43	9.72 $\pm$ 0.44
	intensity	9105	9207 $\pm$ 306	9149 $\pm$ 325	9236 $\pm$ 380
Source 2	x(m)	3	–	3.28 $\pm$ 0.33	3.25 $\pm$ 0.21
	y(m)	50	–	49.63 $\pm$ 0.62	49.73 $\pm$ 0.56
	intensity	1868	–	1806 $\pm$ 157	1901 $\pm$ 164
Source 3	x(m)	41	–	–	40.32 $\pm$ 0.56
	y(m)	5	–	–	5.06 $\pm$ 2.89
	intensity	467	–	–	381 $\pm$ 152

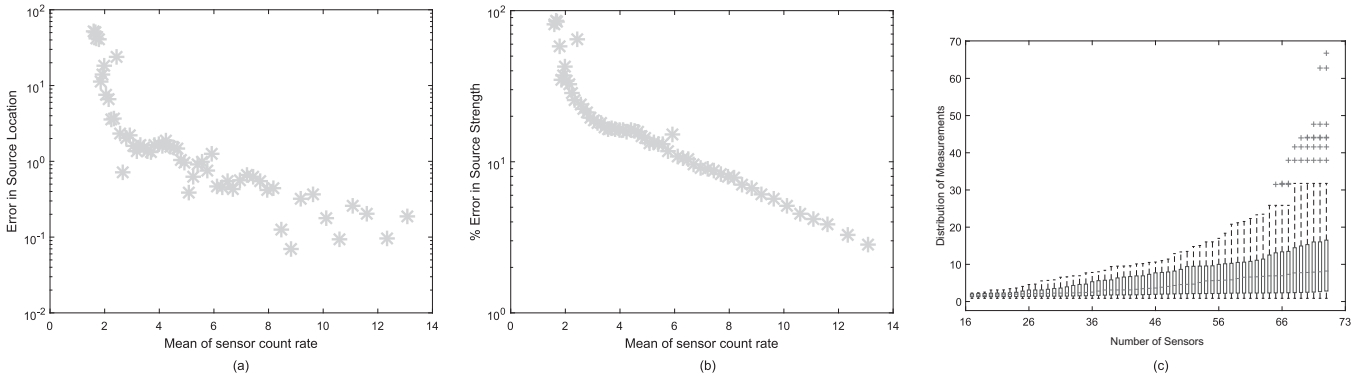

Fig. 11. Test 1: Effect of SNR on source Location and Strength assuming a constant background count of 0.9.(a) Source Location Error vs. Mean Strength of sensors (b) Source Strength Error (%) vs. Mean Strength of sensors (c) Distribution of Sensor readings vs. # of Sensors.

VI. ESTIMATION OF BACKGROUND NOISE

To study the robustness of the proposed SCOPMLE algorithm with respect to the background noise strength, the mean background noise is assumed to be completely unknown and is estimated along other source parameters. Assuming the mean background noise to be constant over the domain of interest as depicted by sensor model of Eq. (1), the mean background noise is appended as additional variable to unknown source parameter vector, $\boldsymbol{\Omega}$. Ideally, we can estimate the background at each sensor location. It will, however, increase the number of variables and one potentially would need to increase the grid points. Table X summarizes the estimated value of different source parameters along with associated uncertainty for all the three test cases. The mean background noise is estimated to be 0.38, 0.21 and 0.32 in case of Test Case 1, Test Case 2, and Test Case 3, respectively. The three tests were carried out on different days. Timing of the tests is what we posit is the reason why the estimated background turned out to be different for the three cases. Although the estimated mean background noise is almost one third of the measured background noise, the true source parameters lie inside one σ box around SCOPMLE estimates. Furthermore, the source parameter estimate are found to vary less than 1% when the mean background noise is varied from 0.1 to 1.0. The negligible variations in estimates of source parameters with respect to variations in assumed mean background noise can be attributed to high signal-to-noise ratio for the collected measurement data. In the next section, we study the effect of signal to noise ratio on the performance of the SCOPMLE algorithm.

A. Effect of Signal to Noise Ratio on the Source Parameter Estimation

To evaluate the performance of the combination of the sparse convex optimization approach which helps identify the number of sources and location of the sources and the Maximum Likelihood Estimator which takes the output of the sparse convex optimization as the initial guess, a series of tasks were performed. Starting with the inclusion of all sensors, the source parameter estimation problem was solved. The following iterate involved dropping the sensor with the largest signal to noise ratio and the source parameters were estimated with a smaller set of sensors. This was repeated until the mean of the remaining sensors had a sensor count rate was about 2 which is nearly twice the background count rate of 0.9.

Fig. 11(a) illustrates the norm of the error in estimated location of the source for the single source case. It can be seen that the error in the estimated location of the source degrades as the mean source strength decreases. The error is smaller than 2 meters for all scenarios where the mean of the sensor count rate was greater than 2. Similarly, Fig. 11(b) illustrates the percent error in the estimate of the source strength. It can be seen that there is a linear degradation (on the log scale) in the estimate of the source strength as the mean of the sensor count rate decreases. The error in the source strength estimates for all sensor suites where the mean of the sensor count rate was greater than 2, ranged between 3 to 30%. To clearly communicate the impact of dropping sensors with the largest SNR, a box and whisker chart is presented in Fig. 11(c). The abscissa corresponds to the number of sensors included in the source

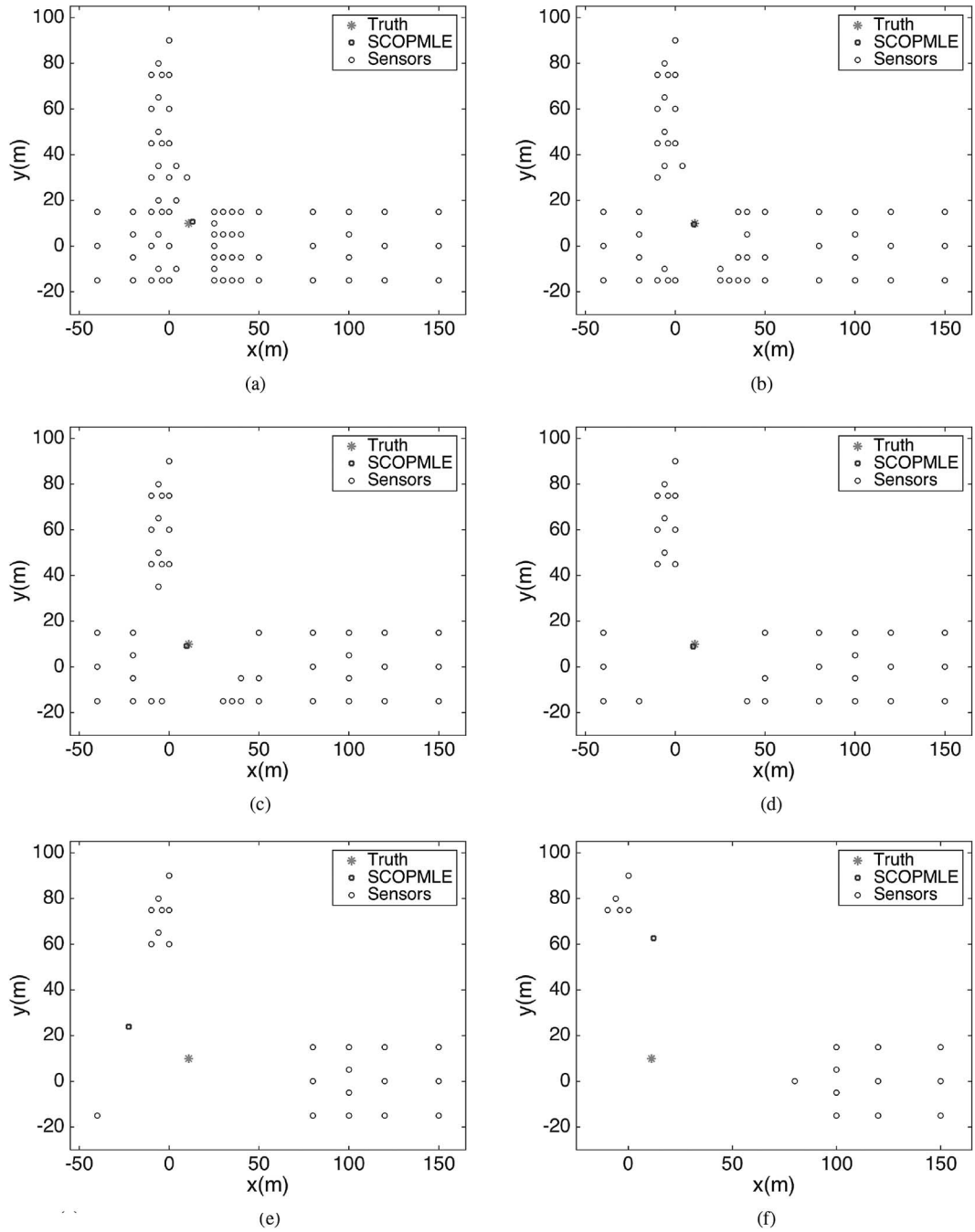

Fig. 12. Sensor Layout (a) Mean Count = 13.0847, Max Count Rate = 66.7833 (b) Mean Count = 9.6227, Max Count Rate = 37.9833 (c) Mean Count = 6.7030, Max Count Rate = 18.3667 (d) Mean Count = 3.049, Max Count Rate = 6.9000 (e) Mean Count = 3.5560, Max Count Rate = 8.000 (f) Mean Count = 1.6115, Max Count Rate = 2.2833.

estimation task. The ordinate represents the distribution of the sensor count rates. This chart clearly illustrates that the performance degradation shown in Figs. 11(a) and 11(b) results from inclusion of sensors, which are farther away from the source and fewer of them. It should be noted that Figs. 11(a) and 11(b) do not capture the impact of the relative location of the sensors, which play a critical role in the localization of the sources. Since the measurement model is a function of the distance of the source from the sensor, the layout of the sensors in relation to the location of the source plays an important role in the ability to localize the source.

Fig. 12 illustrates the sensor layout for six cases ranging from including all sensors to the sensor set when the source localization problem results in erroneous estimates of the source. Information about the mean of the sensor reading and the maximum count rate is also provided since this can be used to gauge the average location of the sensor set and the closest sensor location to the source. It can be seen in Fig. 12(a)–(d), that the source is accurately localized. However, in Figs. 12(e) and (f), it can be seen that the sensor set is smaller and located far from the source. It can also be noted that the sensors are in two clusters, which do not provide enough information to discriminate the

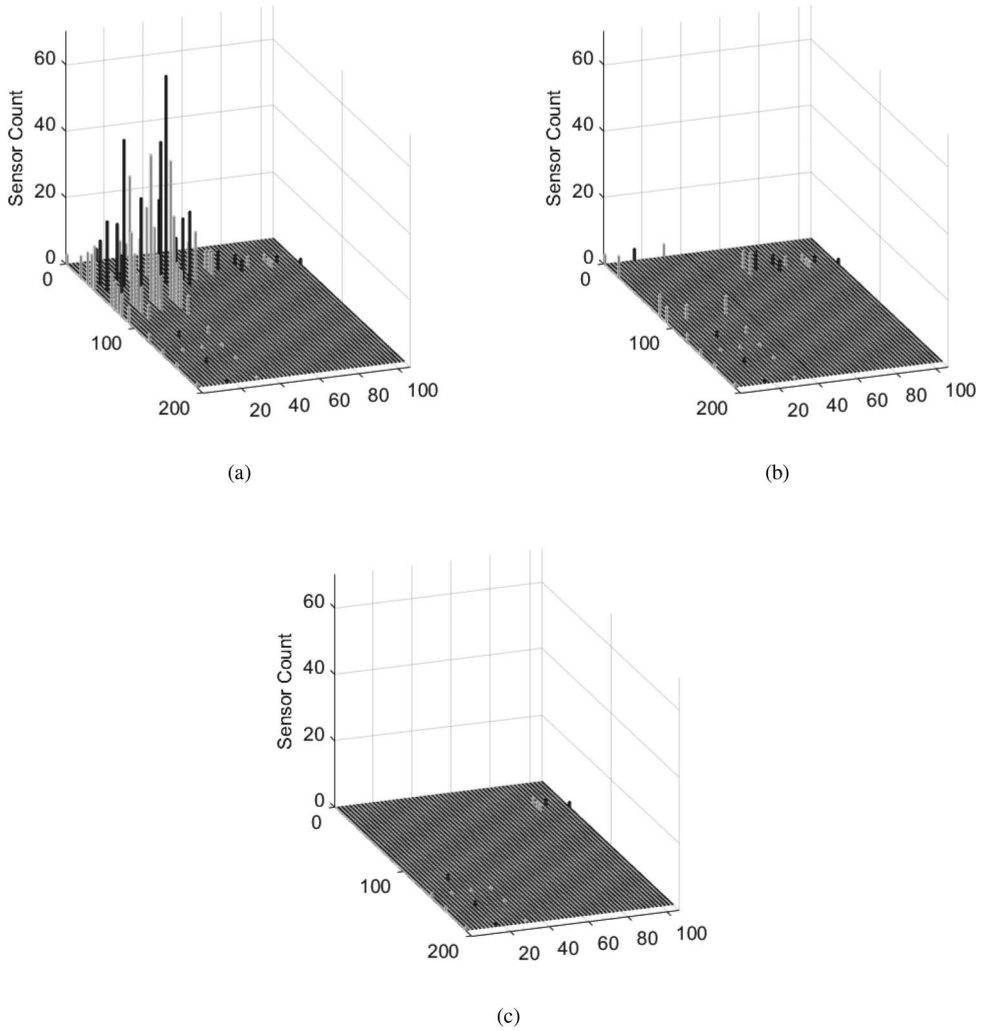

Fig. 13. Test1: Sensor Readings (a) 72 Sensor Readings, (b) 32 Sensor Readings, and (c) 16 Sensor Readings.

source location resulting in a degradation in the performance of the source localization algorithm. For the last case shown in Fig. 12(f), the closest sensor is 65 meters away from the source, while for the case where all the sensor data was used, which corresponds to the case shown in Fig. 12(a), the closest sensor location was 12 meters.

Fig. 13 shows the spatial variation of the magnitude of sensor readings corresponding to three different cases of sensor layouts of Figs. 12(a), 12(d) and 12(f). The x- and y-axis are indices, which correspond to a uniform increment of the sensor locations over a 190×105 meter region. From Figs. 13(a), it can be noted that the maximum sensor count is 66.78, while in Figs. 13(b) and 13(c) the maximum sensor counts are 6.9 and 2.2833, respectively. Fig. 13(b) illustrates that despite weaker readings and fewer sensors compared to the case illustrated in Fig. 13(a), the proposed algorithm localized the source well. Fig. 13(c) corresponds to sensor layout illustrated in Fig. 12(f) where the estimated source parameters did not converge to the truth.

It should be noted that, as shown in Fig. 11(c), the SCOPMLE approach performed reasonably well in the face of simultaneous reduction in the number of sensors and with the resulting sensor suite being located further away from the source. This study concurrently studied the effect of SNR and number of sensors on the ability of the algorithm to correctly identify the number of sources and the source parameters.

The final set of tests involved comparison of the discretization of the spatial domain of interest. The grid size is correlated to number of potential source locations in the $\mathcal{L}_1$ norm optimization problem. The finer the grid size, better is the initial condition for the maximum likelihood estimator part of SCOPMLE. Smaller grid size is also associated with an increased computational cost of the optimization algorithm. Figs. 14(a) and (b) illustrate the source location error and the source strength respectively. Since the benefit of the smaller grid size is noticeable when the sensors are located far from the source, only the results corresponding to fewer sensors located farther away from the source are presented in Fig. 14. The diamonds and the grey asterisx correspond to the results from a coarser and finer gridding of the spatial domain respectively. It should be noted the significant improvement is the estimate of the source strength when fewer sensors which are farther from the source are used to estimate the source parameters.

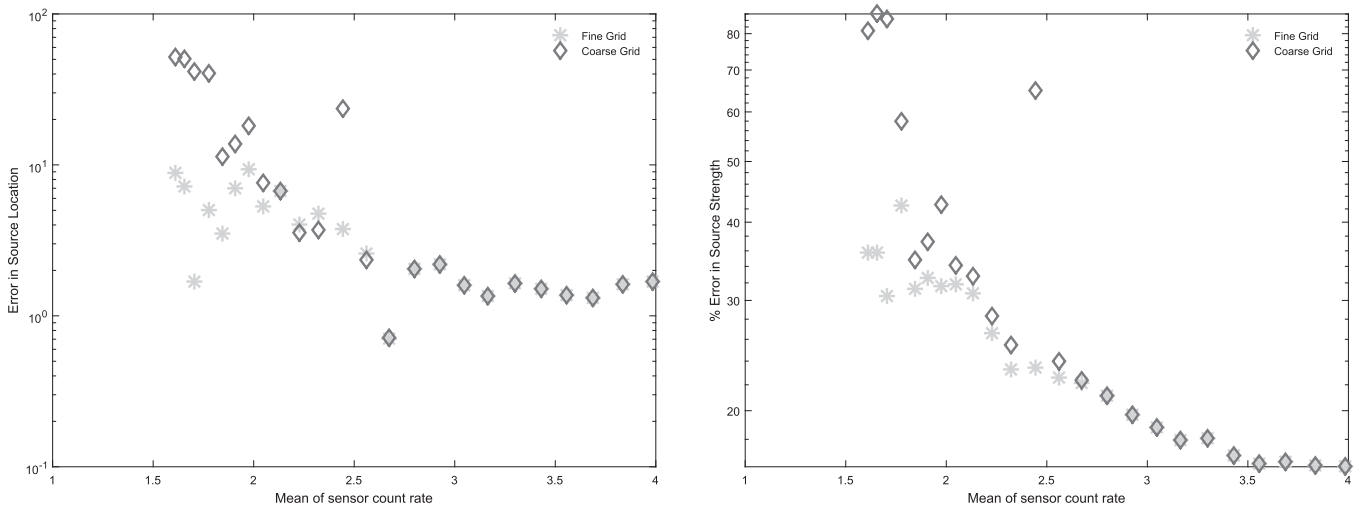

Fig. 14. Test1: Impact of Grid Size (a) Source Location Error and (b) Source Strength Error.

VII. Conclusions

In this paper, a computationally efficient method for the estimation of multiple source parameters such as the number of sources, source locations and intensities was presented. Multiple source term estimation problems pose a unique challenge when the number of sources is unknown. The main contribution of the proposed methodology is that it exploits sparse approximation tools in conjunction with maximum likelihood approach to accurately estimate the number of sources along with other source parameters. The main idea of the proposed approach is to discretize the region of interest where the sources potentially exist and estimate the two-dimensional source intensity distribution directly. First, the discretization procedure brings high efficiency due to the fact that the nonlinear observation model is made formally linear in source intensity and sparse approximation tools based upon recursive $\mathcal{L}_1$-norm minimization is used to provide good estimates for the source intensity. Although the discretization procedure results in large-scale optimization problem, it is solved efficiently by making use of recent advances in convex optimization. A key advantage of the proposed approach is that it handles the model selection problem and the parameter estimation at the same time. Finally, the maximum likelihood estimator is used to further refine the accuracy of the provided estimates. The maximum likelihood estimates guarantee an excellent performance when initially chosen search points are close to the optimal solution. Selecting the source parameters obtained by solving the recursive $\mathcal{L}_1$-norm minimization problem as the initial guess, results in the maximum likelihood estimator improving the accuracy, which was limited by the resolution of the grid. In addition to this, the proposed approach provides uncertainty bounds associated with the source parameter estimates while incorporating sensor model errors. The performance of the proposed algorithm is compared against conventional maximum likelihood estimator and important sampling with progressive correction by making use of three different datasets corresponding to real experiments involving three sources of different strengths. The results presented illustrate that the proposed approach performs well in providing estimates of source parameters along with the uncertainties associated with these estimates. To evaluate the impact of the SNR, a series of problems were solved where the strongest sensor reading was eliminated from the data set, which resulted in fewer sensor reading with smaller SNRs. It was shown that the source strength estimates and the source location estimate errors grew monotonically with smaller SNRs.

Acknowledgment

This material is based upon work jointly supported through National Science Foundation (NSF) under Awards No. CMMI-1054759 and Office of Naval Research (ONR) grant number HM1582-08-1-0012. All results and opinions expressed in this article are those of the authors and do not reflect opinions of the NSF or ONR.

References

[1] IAEA "Trafficking in nuclear and radioactive material in 2005," http://www.iaea.org/NewsCenter/News/2006/traffickingstats2005., 2006.
[2] WHO/REMPAN "The radiological accident in lilo," Georgia http://helid.desastres.net/en/d/Js2993e/9.3, 2002.
[3] B. K. Sovacool, "A preliminary assessment of major energy accidents," *Energy Policy*, vol. 36, pp. 1802–1820, 2008.
[4] B. K. Sovacool, "A critical evaluation of nuclear power and renewable electricity in asia," *J. Contemporary Asia*, vol. 40, no. 3, pp. 393–400, 2010.
[5] Y. Qin and K. Oduyemi, "Atmospheric aerosol source identification and estimates of source contributions to air pollution in Dundee, UK," *Atmospheric Environment*, vol. 30, pp. 579–587, 1996.
[6] B. Deb, "Iterative estimation of location and trajectory of radioactive sources with a networked system of detectors," *IEEE Trans. Nucl. Sci.*, vol. 60, no. 2, pp. 1315–1326, 2013.
[7] J. W. Howse, L. O. Ticknor, and K. R. Muske, "Least squares estimation techniques for position tracking of radioactive sources," *Automatica*, vol. 37, no. 11, pp. 1727–1737, 2001.
[8] C. T. Allen, G. S. Young, and S. E. Haupt, "Improving pollutant source characterization by better estimating wind direction with a genetic algorithm," *Atmospheric Environment*, vol. 41, no. 11, pp. 2283–2289, 2007.

[9] M. Morelande, B. Ristic, and A. Gunatilaka, "Detection and parameter estimation of multiple radioactive sources," *Proc. 10th Int. Conf. Inform. Fusion (FUSION), 2007*, 2007, pp. 1–7.
[10] R. J. Nemzek, J. S. Dreicer, D. C. Torney, and T. T. Warnock, "Distributed sensor networks for detection of mobile radioactive sources," *IEEE Trans. Nucl. Sci.*, vol. 51, no. 4, pp. 1693–1700, Aug. 2004.
[11] A. Gunatilaka, B. Ristic, and M. Morelande, "Experimental verification of algorithms for detection and estimation of radioactive sources," *Proc. 13th Int. Conf. Inform. Fusion (FUSION), 2010*, 2010, pp. 1–8.
[12] M. R. Morelande and B. Ristic, "Radiological source detection and localisation using bayesian techniques," *IEEE Signal Process. Mag.*, vol. 57, no. 11, pp. 4220–4231, 2009.
[13] C. Musso, N. Oudjane, and F. Gland, "Improving regularised particle filters," *Sequential Monte Carlo Methods in Practice*, A. Doucet, N. Freitas, N. Gordon, Eds. New York: Springer, 2001, pp. 247–271, Statistics for Engineering and Information Science.
[14] C. E. Shannon, "A mathematical theory of communication," *Bell Syst. Tech. J.*, vol. 27, pp. 379–423–623–656, 1948.
[15] G. Schwarz, "Estimating the dimension of a model," *The Ann. of Statist.*, vol. 6, no. 2, pp. 461–464, 1978.
[16] J. B. Kadane and N. A. Lazar, "Methods and criteria for model selection," *J. Amer. Statist. Assoc.*, vol. 99, no. 465, pp. 279–290, 2004.
[17] U. Konda, Y. Cheng, T. Singh, and P. Scott, "Source estimation in CBRN incidents using convex optimization," *Proc. Chem. and Biol. Defense Phys. Sci. & Technol. Conf.*, New Orleans, Louisiana: Nov. 2008.
[18] Y. Cheng and T. Singh, "Source term estimation using convex optimization," *Proc. 11th Int. Conf. Inform. Fusion (FUSION), 2008*, Cologne, Germany: Jul. 2008.
[19] M. Grigoriu, *Stochastic Calculus Applications in Science and Engineering*, Basel: Birkhauser Verlag, 2002.
[20] G. Christakos, *Random Field Models in Earth Sciences*, Academic Press, 1992.
[21] E. T. Jaynes, *Probability Theory, the Logic of Science*, Cambridge University Press, 2003.
[22] G. F. Knoll, *Radiation Detection and Measurement*, 2nd Ed. New York, NY: John Wiley & Sons, 1988, chapter 3.
[23] S. M. Brennan, A. M. Mielke, D. C. Torney, and A. B. Maccabe, "Radiation detection with distributed sensor networks," *IEEE Computer*, vol. 37, no. 8, pp. 57–59, Aug. 2004.
[24] S. Chen and D. Donoho, "Atomic decomposition by basis pursuit," *Proc. SPIE Int. Conf. Wavelets*, Jul. 1995.
[25] S. Mallat and Z. Zhang, "Matching pursuits with time-frequency dictionaries," *IEEE Trans. Signal Process.*, vol. 41, no. 12, 1993.
[26] E. J. Candès, "Compressive sampling," *Proc. Int. Congress of Math.: Madrid, Aug. 22–30, 2006*, pp. 1433–1452, 2006, invited lectures.
[27] S. Boyd and L. Vandenberghe, *Convex Optimization*, Cambridge, U.K.: Cambridge University Press, 2004.
[28] D. L. Donoho, Y. Tsaig, I. Drori, and J.-L. Starck, "Sparse solution of underdetermined systems of linear equations by stagewise orthogonal matching pursuit," *IEEE Trans. Inform. Theory*, vol. 58, no. 2, pp. 1094–1121, 2012.
[29] E. J. Candès, M. B. Wakin, and S. Boyd, "Enhancing sparsity by reweighted l1 minimization," *J. Fourier Anal. and Appl.*, vol. 14, no. 5, pp. 877–905, 2008.
[30] S. Kullback, *Inform. Theory and Statist.*, Dover Publications, 1997.
[31] A. Gunatilaka, B. Ristic, and M. Morelande, "Experimental verification of algorithms for detection and estimation of radioactive sources," *Proc. 13th Int. Conf. Inform. Fusion (FUSION), 2010*, Jul. 2010, pp. 1–8.
[32] M. Grant and S. Boyd, "CVX: Matlab software for disciplined convex programming," http://cvxr.com/cvx/ (web page and software)